공학박사 학위논문

Development of instrumented indentation test model for fracture toughness evaluation and cryogenic test application

파괴인성 평가를 위한 연속압입시험 모델 개발 및 극저온 시험 응용

2020년 7월

서울대학교 대학원

재료공학부

김 우 주

Development of instrumented indentation test model for fracture toughness evaluation and cryogenic test application

파괴인성 평가를 위한 연속압입시험 모델 개발 및 극저온 시험 응용

지도교수 권 동 일

이 논문을 공학박사 학위논문으로 제출함
2020년 7월

서울대학교 대학원
재료공학부
김 우 주

김우주의 박사 학위논문을 인준함
2020년 7월

위 원 장 _____

부위원장 _____

위 원 _____

위 원 _____

위 원 _____

Abstract

Kim, Woojoo
Dept. of Materials Science and Engineering
The Graduate School
Seoul National University

Structural integrity assessment is to evaluate the condition of a structure or component before it is destroyed. To manage the structural integrity, an engineer must consider the presence of flaws, designed stress and material properties in the structures. But the most important factor is the mechanical properties of a material firstly, such as strength, hardness, or fracture toughness. In many cases, structural failures arise from the change of mechanical properties of the material due to degradation or embrittlement so that it is required to, if possible, measure in-situ mechanical properties of in-service structural components for structural integrity assessment.

There are various mechanical properties, however, among them, fracture toughness, the resistance to crack propagation, is one of the most important mechanical properties for fracture mechanical analysis on structural integrity. But the standard fracture toughness test is a

destructive method and requires complex shapes and test procedures, making it nearly impossible to measure the fracture toughness of an in-service structures. For this reason, a nondestructive tool to measure in-situ mechanical properties as well as fracture toughness has required and developed to improve the reliability of structural integrity assessment.

Instrumented indentation testing can be considered one of solutions in this issue because it is developed for nondestructive testing of in-field structures. Many researchers have worked to estimate fracture toughness of metallic materials using instrumented indentation testing, trying to develop theoretical or experimental models. The study on the prediction of fracture toughness through the instrumented indentation test started from methods of generating cracks, but the study on the metallic materials that does not occur crack was expanded. In the fact that the crack does not occur in the metallic material, the study has been divided into mechanical model and fracture energy model, but in both cases, many assumptions and empirical correlations have been used.

In this study, indentation fracture toughness models are introduced. Among them, flat tip fracture toughness estimation model is selected due to its simple test method and derivation of the fracture mechanics situation. Since the previous approach was focused on being somehow

phenomenal in the method of determining fracture toughness, this approach was tired to determine the fracture toughness in an indentation situation by adapting fracture mechanics. According to fracture mechanisms, two distinct indentation fracture toughness models, ductile fracture model and brittle fracture model, are modified. In ductile fracture model, in order to match the stress state beneath an indenter with that ahead of a crack tip, fully plastic state at fracture in ligament of cracked round bar test specimen, crack initiation point is determined at the point which fully plastic zone is developed beneath the indenter. In brittle fracture, it is noted that brittle fracture does not involve plasticity, and the crack initiation point in the indentation test is determined using small scale yielding condition at which plastic deformation energy is minimal.

By using the flat punch indenter, due to the geometry of the indenter, one normalized curve not dependent on the size of indenter radius can be obtained and this can be converted to any other sized indentation load-depth curve. Thus, for those two model, the indenter size with a radius corresponding to 1T thickness can be determined, and the fracture toughness can be calculated from the load-displacement curve of that size.

To verify developed models, experimental results are compared with standard J test results and it is confirmed that these results match well

within 20% error range in both two models.

In addition, since, it is very important in practical structures to ensure fracture toughness at cryogenic temperatures, cryogenic indentation system was developed. The system was designed and improved by referring to the previous environmental indentation test and conventional environmental facilities. The developed system was applied to materials used in nuclear power plant structures, and compared with the fracture toughness values obtained from the master curve method.

Keywords: Instrumented Indentation Testing, Fracture Toughness, Flat Punch, Ductile Fracture, Brittle Fracture, Cryogenic indentation

Student Number: 2013-20589

CONTENTS

LIST OF TABLES

LIST OF FIGURES

Figure 2.10
Schematic of typical stress-stain curves: (a) brittle material and (b) ductile material

Figure 2.11
Schematic diagram of typical load-depth curve obtainable during instrumented indentations: (a) Sharp indentation and (b) Spherical indentation

Figure 2.12
Variation of indentation loading curves with changes in the stress state

Figure 2.13
Theoretical surface morphologies around the contact for (a) stress-free, (b) tensile stress, and (c) compressive stress states

Figure 2.14
Crack system for Vickers indenter: (a) radial cracks, (b) lateral cracks, (c) median cracks, and (d) half-penny cracks [102]

Figure 2.15
Schematic of radial cracking by Vickers indentation

Figure 2.16
Decreasing elastic modulus with indentation depth (API steels)

Figure. 2.17
Schematic diagram of expanding cavity model

Figure 2.18
The concept of flat indentation fracture toughness: Geometrical similarity between flat punch indentation and CRB fracture toughness test. [88]

Figure 2.19

Chapter 1

INTRODUCTION

Contents

1.1. Objective of the Thesis

Structural integrity is the ability of a structure or a component to withstand a designed service load, resisting structural failure due to fracture, deformation, or fatigue. It is a concept often used in engineering, to produce items that will not only function adequately for their designed purposes, but also to function for a desired service life. To construct an item with structural integrity, an engineer must first consider the mechanical properties of a material, such as strength, hardness, or fracture toughness, and then determine a suitable size, thickness, or shape that will withstand the desired load for a long life. In many cases, structural failures arise from the change of mechanical properties of the material due to degradation or embrittlement so that it is required to, if possible, measure in-situ mechanical properties of in-service structural components for structural integrity assessment.

Fracture toughness, which is defined as the resistance to crack propagation, is one of the most important mechanical properties for fracture mechanical analysis on structural integrity. Several fracture toughness parameters are available according to given mechanical situations or testing methods, including the critical stress intensity factor,

K_{IC}, the critical value of the J-integral, J_{IC}, and the critical crack-tip opening displacement, CTOD or δ_{IC}. But these fracture toughness parameters are largely influenced by testing variables such as specimen geometry, crack length, constraint, temperature, strain rate, so that testing and determining fracture toughness parameters are complex and difficult. Moreover, since standard fracture toughness testing also has destructive nature of conventional mechanical testing and requires many specimen with specified geometry, measuring in-situ fracture toughness on in-service structural components is almost impossible. For this reason, a nondestructive way to measure in-situ mechanical properties as well as fracture toughness has required and developed to improve the reliability of structural integrity assessment.

Instrumented indentation testing can be considered one of solutions in this issues, which is developed for nondestructive testing of in-field structures. This technique can be used to measure various mechanical properties such as hardness, elastic modulus [1-3], tensile properties [4-17], residual stress [18-22], and fracture toughness [23-32] by analyzing the indentation load-depth curve. This testing makes just a little indent on the surface of the material so that it can be applied for in-situ and in-field measurement as nondestructive mechanical testing and for mechanical

mapping by local area testing in multi scale level.

A well-known technique to evaluate fracture toughness using instrumented indentation testing is so-called ‘indentation cracking method’, which used relationship between an indentation-induced crack length, an indentation load and indentation parameters [23-27]. This method can be applied for very brittle materials like ceramics that cracking occur during indentation. However, in case of ductile materials like metals as structural materials, cracking does not occur during indentation, so that the indentation cracking method is not appropriate for nondestructive structural integrity assessment of such materials. Consequently, many researchers have worked to estimate fracture toughness of metallic materials using instrumented indentation testing, trying to develop theoretical or experimental models [28-32]. But these studies have some difficulties arising from many assumptions and empirical correlations as an inevitable consequence of estimation from non-cracking to cracking resistance, that is, fracture toughness.

In this study, improved fracture toughness models is developed by more theoretical and practical approaches based on fracture mechanics and contact mechanics to estimate fracture toughness of metallic materials. First, in order to match the stress state beneath an indenter with that

ahead of a crack tip, a flat punch indenter is selected instead of a spherical indenter which is generally used in indentation techniques. By using the flat punch indenter, crack-like stress concentration is derived at the edge of the indenter tip. Second, from this, the concept of modeling is designed as deriving virtual fracture toughness from flat punch indentation, not as conventional methods of correlating indentation deformation energy with fracture energy. Finally, cryogenic indentation system was developed. By using cryogenic indentation system, indentation fracture toughness was evaluated in cryogenic environment and then, changes of fracture toughness was observed.

1.2. Outline of the Thesis

The thesis has six chapters. After a brief introduction in Chapter 1, Chapter 2 gives a historical overview of fracture mechanics, stress analysis of cracks, fracture toughness parameters, and methods to measure fracture toughness. Theories and methods for Instrumented Indentation Technique (IIT), a nondestructive technique to evaluate mechanical properties such as hardness, elastic modulus, tensile properties, residual stress, and fracture toughness are discussed in details, in particular previous work on fracture toughness. Modified modeling to estimate fracture toughness is presented in Chapter 3. In Chapter 4, experimental works to verify developed models is described and the results are discussed. Development of cryogenic indentation system is described in Chapter 5. Cryogenic experiments were performed on materials used in nuclear structures using a cryogenic temperature system and the results were compared with the master curve. Finally, conclusions are given in Chapter 6.

Chapter 2

RESEARCH BACKGROUND

Contents

2.1. Fracture mechanics

Strength failures of load bearing structures can be either of the yielding dominant failures or fracture dominant failures. Defects are important for both failures, but those of primary importance to fracture differ in an extreme way from those influencing yielding and the resistance to plastic flow. These differences are illustrated schematically in Fig 2.1 [33].

For yielding dominant failures the significant defects are those which tend to warp and interrupt the crystal lattice planes, thus interfering with dislocation glide and providing a resistance to plastic deformation that is essential to the strength of high strength metals. Examples of such defects are interstitial and out-of-size substitutional atoms, grain boundary, coherent precipitates and dislocation networks. Larger defects like inclusions, porosity, surface scratches and small cracks may influence the effective net section bearing the load, but otherwise have little effect on resistance to yielding.

For fracture dominant failures, the size scale of the defects which are of major significance is essentially macroscopic, since general plasticity is not involved but only the local stress-strain fields associated with the defects. The minute lattice-related defects which control resistance to

plastic flow are not of direct concern. They are important insofar as the resistance to plastic flow is related to the material's susceptibility to fracture.

2.1.1. Overview

The commonly accepted first successful analysis of a fracture dominant problem was that of the Griffith in 1920 [34], who considered the propagation of brittle cracks in glass. Griffith formulated the well-known concept that an existing crack will propagate if thereby the total energy of the system is lowered, and he assumed that there is a simple energy balance, consisting of a decrease in elastic strain energy within the stressed body as the crack extends, counteracted by the energy needed to create the new crack surface. From Griffith theory [34], fracture stress is obtained like in Eq. (2-1),

$$\sigma = \left(\frac{2E\gamma_s}{\pi a}\right)^{\frac{1}{2}} \tag{2-1}$$

where, a is crack length and $2\gamma_s$ is surface energy. Eq. (2-1) indicates

that crack extension in ideally brittle materials is governed by the product of the remotely applied stress and the square root of the crack length and by material properties. Because E and γ_s are material properties the right-hand side of Eq. (2-1) except the crack length, a, is equal to a constant value characteristic of a given ideally brittle material. Consequently, Eq. (2-1) indicates that crack extension occurs when the product $\sigma\sqrt{a}$ attains a certain critical value. The Griffith concept has some limitations which it was only elastic, brittle materials, in which no plastic deformation took place.

So Irwin [35] modified the Griffith expression to account for ductile material. Irwin indicated that the Griffith energy balance must be between the stored strain energy and the surface energy plus the work done in plastic deformation. He recognized that for relatively ductile materials the energy required to form new crack surfaces is generally insignificant compared to the work done in plastic deformation. The revised expression is given by,

$$\sigma_f = \left(\frac{2E\left(\gamma_s + \gamma_p\right)}{\pi a}\right)^{\frac{1}{2}} \qquad (2\text{-}2)$$

where γ_p is the plastic work per unit area of surface created, and is typically much larger than γ_s. He also defined a quantity which is called energy release rate or crack driving force, *G*, as the total energy that is released during cracking per unit increase in crack size. Moreover, Irwin contributed another major advance by showing that the energy approach (*G*) is equivalent to a stress intensity approach (*K*), according to which fracture occurs when a critical stress distribution ahead of the crack tip is reached, which a critical strain energy release rate (G_c) or critical stress intensity (K_c) is accomplished.

In 1960s, fracture mechanics theories have been developed to account for various type of nonlinear material behavior, i.e. plasticity, notably Well's [36] work on Crack Tip Displacement (COD). In 1968, Rice [37] introduced an elastic-plastic fracture parameter with a more theoretical basis: J integral, which the energy release rate can be expressed as a path-independent line integral. Although both COD and J are now well established concepts, Elastic-Plastic Fracture Mechanics (EPFM) is still very much an evolving discipline. The reason is the greater complexity of elastic-plastic analysis.

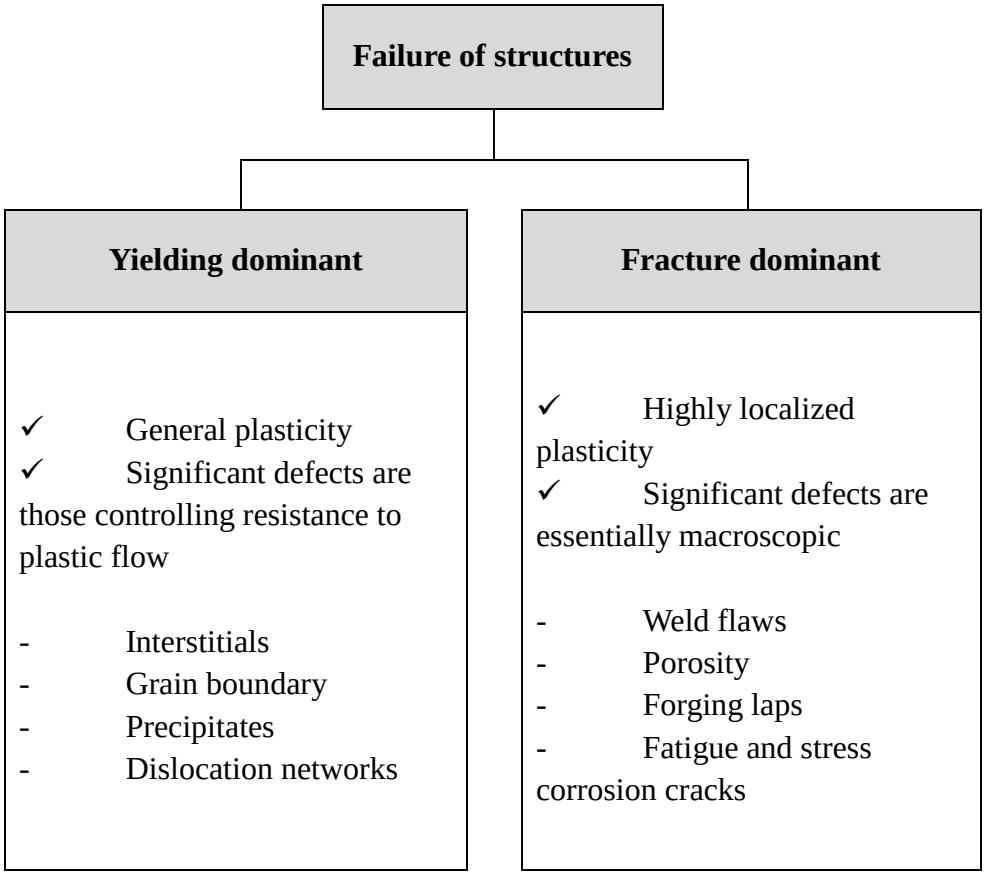

Fig. 2.1 Type of structural failure [33]

2.1.2. Stress analysis of cracks

2.1.2.1. Crack tip stress analysis

There are three types of loading that a crack can experience, as Fig.2.2 illustrates. Mode I loading where the principle load is applied normal to the crack plane, tends to open the crack. The two fracture surfaces are displaced perpendicular to each other in opposite directions. Mode II corresponds to in-plane shear loading and tends to slide one crack face with respect to the other. Mode III refers to out-of-plane shear. A cracked body can be loaded in any one of these modes, or a combination of two or three modes.

Westergaad [38] and Irwin [39] developed analytically the crack tip stress field for a linear elastic isotropic material subjected to the three modes of deformation, and they are listed in Table 2.1. The stress components and the coordinates r and θ are shown in Fig. 2.3; u_x, u_y, and u_z are the displacements in the x, y, and z directions, respectively; v is Poisson's ratio, and G is the shear modulus of elasticity.

2.1.2.2. Effect of constraint on fracture toughness

Of the three primary factors that affect the fracture toughness of a given material; that is, temperature, loading rate, and constraint, the effect of constraint is the most difficult to establish quantitatively. The primary definition of constraint deals with the plane strain to plane stress transition as defined by specimen thickness. Plane strain refers to maximum constraint and occurs in very thick test specimens that have deep cracks. In contrast, plane stress refers to minimum constraint and occurs in thin test specimens.

Ahead of sharp crack, the lateral constraint which increases with increasing specimen thickness is such that through-thickness stresses are present. Because these through-thickness stresses must be zero at each surface of a specimen, they are less for thin specimens compared with thick them. For very thick specimens, the through-thickness stresses at the centerline are large, and a triaxial tensile state of stress occurs ahead of the crack. This triaxial state of stress reduces the apparent ductility of the material by decreasing the shear stresses. Because yielding is restricted, the constraint ahead of the crack is increased and thus the fracture toughness is reduced. This decrease in fracture toughness is

controlled by the thickness of the specimen, even though the inherent metallurgical properties of the material may be unchanged. Thus, the fracture toughness is smaller for thick specimens compared with thinner specimens of the same material. This behavior is shown schematically in Fig. 2.4 [40], which indicates that the minimum fracture toughness of a particular material, K_{IC}, is reached when the thickness of the specimen is large enough so that the state of stress is plane strain.

To demonstrate the significant constraint effect on the fracture behavior of a given material, it can be consider a point on the crack plane just ahead of the crack tip. According to Table 2.1, the stresses in the x and y direction a point on the crack plane ($\theta = 0$) for Mode I are equal:

$$\sigma_x = \sigma_y = \frac{K_I}{\sqrt{2\pi r}} \tag{2-3}$$

When $\theta = 0$ under linear elastic conditions, the shear stress is zero, which means that the crack plane is a principal plane for pure Mode I loading. If the stress state is the plane stress, $\sigma_z = 0$ by definition. Under plane strain conditions, $\sigma_z = 2\nu\sigma_y$. Substituting these stresses into the von Mises yield criterion leads to the following:

$$\sigma_y = \sigma_{ys} \text{ (plane stress)} \quad (2\text{-}4a)$$

$$\sigma_y = 2.5\sigma_{ys} \text{ (plane strain)} \quad (2\text{-}4b)$$

assuming $\nu = 0.3$. Therefore, the triaxial stress state associated with plane strain leads to higher stresses in the plastic zone. For fracture mechanisms that are governed by normal stress, such as cleavage in metals, the material will behave in a more brittle fashion when subjected to a triaxial stress state. Triaxial stresses also assist ductile fracture process such as microvoid coalescence.

Pellini [41] described the physical significance of constraint and plate thickness on fracture toughness in terms of plastic flow, as shown in Fig. 2.5. This Fig. shows that the introduction of a circular notch in a bar loaded in tension causes an elevation of the stress-strain curve. The plastic flow of the smooth tensile bar, which is usually used to develop conventional stress-strain curves, is free flow because lateral contraction is not constrained during initial loading. In the notched bar, however, the reduced section deforms inelastically while the ends of the specimen are still loaded elastically. Since the amount of elastic contraction is small compared to the inelastic contraction of reduced section, a restriction to plastic flow is developed. This restriction is in the nature of a reaction-

stress system such that the σ_x and σ_y stresses restrict or constrain the flow in the σ_y direction. Thus, the uniaxial stress state of the smooth bar is changed to a triaxial tensile stress system in the notched bar compared with the unnotched bar. As the notch becomes far sharper, the severity of the stress state increases.

Table 2.1 Stress and displacement fields ahead of crack tip for each mode

	Mode I	**Mode II**	**Mode III**
σ_{xx}	$\frac{K_I}{\sqrt{2\pi r}}\cos\left(\frac{\theta}{2}\right)\left[1-\sin\left(\frac{\theta}{2}\right)\sin\left(\frac{3\theta}{2}\right)\right]$	$\frac{K_{II}}{\sqrt{2\pi r}}\sin\left(\frac{\theta}{2}\right)\left[2+\cos\left(\frac{\theta}{2}\right)\cos\left(\frac{3\theta}{2}\right)\right]$	-
σ_{yy}	$\frac{K_I}{\sqrt{2\pi r}}\cos\left(\frac{\theta}{2}\right)\left[1+\sin\left(\frac{\theta}{2}\right)\sin\left(\frac{3\theta}{2}\right)\right]$	$\frac{K_{II}}{\sqrt{2\pi r}}\sin\left(\frac{\theta}{2}\right)\cos\left(\frac{\theta}{2}\right)\cos\left(\frac{3\theta}{2}\right)$	-
σ_{zz}	0 (plane stress) $\nu(\sigma_{xx}+\sigma_{yy})$ (plane strain)	0 (plane stress) $\nu(\sigma_{xx}+\sigma_{yy})$ (plane strain)	-
τ_{xy}	$\frac{K_I}{\sqrt{2\pi r}}\cos\left(\frac{\theta}{2}\right)\sin\left(\frac{\theta}{2}\right)\cos\left(\frac{3\theta}{2}\right)$	$\frac{K_{II}}{\sqrt{2\pi r}}\cos\left(\frac{\theta}{2}\right)\left[1-\sin\left(\frac{\theta}{2}\right)\sin\left(\frac{3\theta}{2}\right)\right]$	-
τ_{yz}	0	0	$\frac{K_{III}}{\sqrt{2\pi r}}\cos\left(\frac{\theta}{2}\right)$
τ_{xz}	0	0	$-\frac{K_{III}}{\sqrt{2\pi r}}\sin\left(\frac{\theta}{2}\right)$
u_x	$\frac{K_I}{2\mu}\sqrt{\frac{r}{2\pi}}\cos\left(\frac{\theta}{2}\right)\left[\kappa-1+2\sin^2\left(\frac{\theta}{2}\right)\right]$	$\frac{K_{II}}{2\mu}\sqrt{\frac{r}{2\pi}}\sin\left(\frac{\theta}{2}\right)\left[\kappa+1+2\cos^2\left(\frac{\theta}{2}\right)\right]$	-
u_y	$\frac{K_I}{2\mu}\sqrt{\frac{r}{2\pi}}\sin\left(\frac{\theta}{2}\right)\left[\kappa+1-2\cos^2\left(\frac{\theta}{2}\right)\right]$	$-\frac{K_{II}}{2\mu}\sqrt{\frac{r}{2\pi}}\cos\left(\frac{\theta}{2}\right)\left[\kappa-1-2\sin^2\left(\frac{\theta}{2}\right)\right]$	-
u_z	-	-	$\frac{2K_{III}}{\mu}\sqrt{\frac{r}{2\pi}}\sin\left(\frac{\theta}{2}\right)$

Note: ν is Poisson's ratio and μ is the shear modulus. $\kappa = 3 - 4\nu$ (plane strain) and $\kappa = (3- \nu) / (1+ \nu)$ (plane stress).

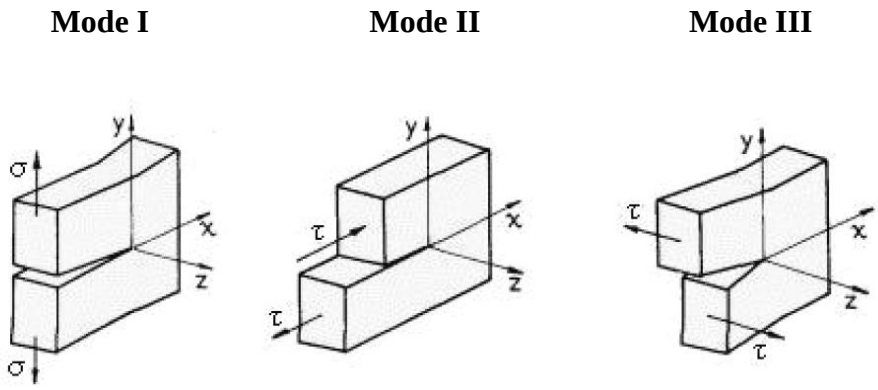

Fig. 2.2 The three modes of loading that can be applied to a crack

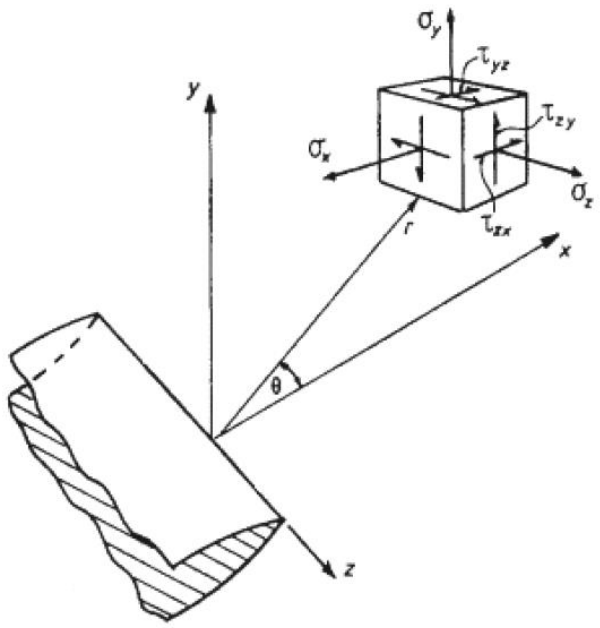

Fig. 2.3 Coordinate system and stress components ahead of crack tip

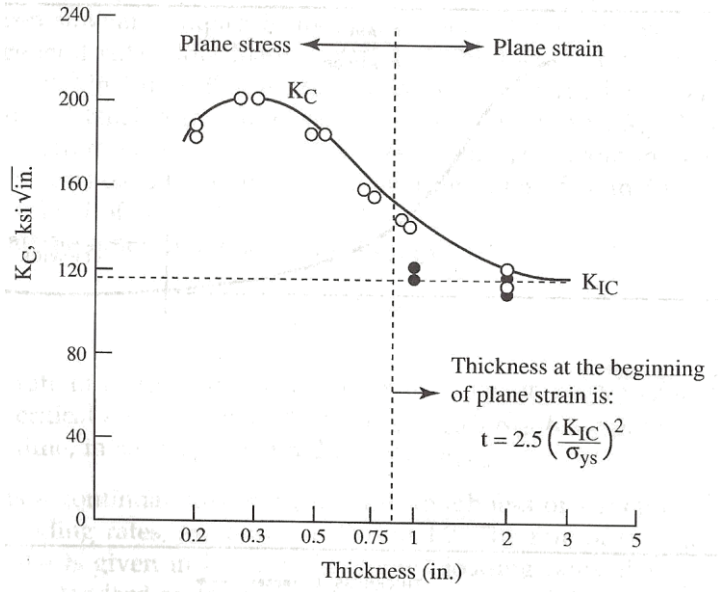

Fig. 2.4 Effect of thickness on Kc behavior [40]

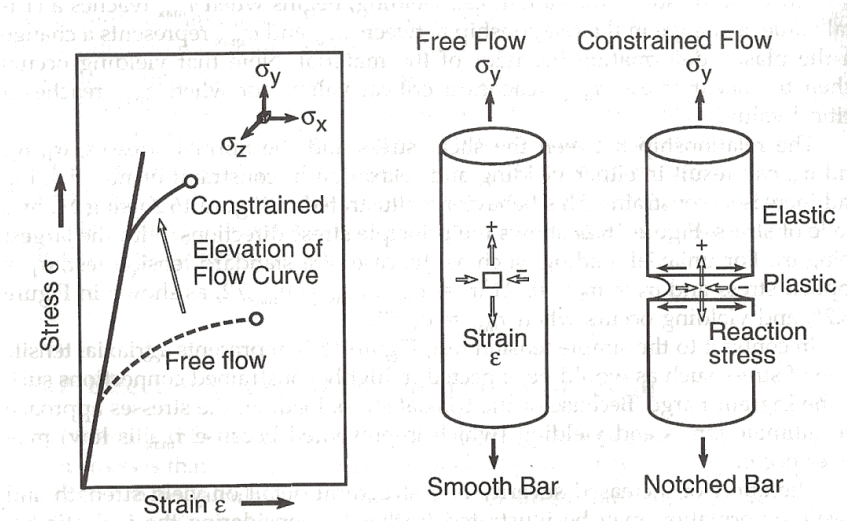

Fig. 2.5 Constraint to plastic flow caused by notched geometries [40]

2.1.3. Fracture toughness parameters

The fracture toughness of a material measures its ability to resist crack initiation and propagation. Several fracture toughness parameters available, including critical stress intensity factor, the critical value of the J integral, and the critical crack tip opening displacement.

2.1.3.1. Stress intensity factor

Irwin [39] showed that the stresses in the vicinity of a crack tip take the form

$$\sigma_{ij} = \frac{K}{\sqrt{2\pi r}} f_{ij}(\theta) + \cdots \quad (2\text{-}5)$$

where r, θ are the cylindrical polar coordinates of a point with respect to the crack tip. K is a quantity which gives the magnitude of the elastic stress field. It is called the stress intensity factor. Dimensional analysis shows that K must be linearly related to stress and directly related to the square root of a characteristic length. Eq. (2-1) from Griffith analysis indicates that this characteristic length is the crack length, and it turns out

that the general form of the stress intensity factor is given by:

$$K = \sigma\sqrt{\pi a} \cdot f(a/W) \quad (2\text{-}6)$$

where *f(a/W)* is a dimensionless parameter that depends on the geometries of the specimen and crack, and σ is the applied stress.

It is customary to write the limiting value of K for maximum constraint, i.e. plane strain, in Mode I fracture as K_{IC}. K_{IC} can be considered a material property characterizing the crack resistance, and is therefore called the plane strain fracture toughness. Thus the same value of K_{IC} should be found by testing specimen of the same material with different geometries and with critical combinations of crack size and shape and fracture stress.

2.1.3.2. Crack tip opening displacement

Wells [42] focuses on the strains in the crack tip region instead of the stresses, unlike the stress intensity approach. He noticed that the crack faces had moved apart prior to fracture; In the presence of the plasticity, i.e. plastic deformation, had blunted an initially sharp crack. The degree of crack blunting increased in proportion to the toughness of the material,

as illustrated in Fig. 2.6. Eventually, Wells proposed to use the crack flank displacement at the tip of a blunting crack, the well-known the Crack Tip Opening Displacement (CTOD) as a measure of fracture toughness parameter.

There are a number of alternative definitions of CTOD. The two most common definitions, which are shown in Fig. 2.7, are the displacement at the original crack tip and the 90^{o} intercept. These two definitions are equivalent if the crack blunts in a semicircle.

CTOD can be considered as a strain-based estimate of fracture toughness. However, it can be separated into elastic and plastic components, which is displayed in Eq. (2-7).

$$\delta = \delta_{el} + \delta_{p}. \tag{2-7}$$

The subscripts el and p denote elastic and plastic components, respectively.

The elastic part of CTOD is derived from the stress intensity factor computed by the load and specimen dimensions, K. In some standards, the plastic component of CTOD is obtained by assuming that the specimen rotates about a plastic hinge like in Fig. 2.8 [43]. The plastic

component is derived from the crack mouth opening displacement which measured using a clip gauge. The position of the plastic hinge is given in test standards for each specimen type.

2.1.3.3. J-Integral

The fracture parameter J-integral proposed by Rice [37] means a contour integral that can be evaluated along any arbitrary path enclosing the crack tip, as illustrated in Fig. 2.9. Rice considered the potential energy changes involved in crack growth in non-linear elastic material. Such non-linear elastic behavior is a realistic approximation for plastic behavior provided no unloading occurs in any part of the material. From these concepts, Rice derived J-integral. J is derived from the Eq. (2-8):

$$J = \int_{\Gamma} \left(w dy - T_i \frac{\partial u_i}{\partial x} ds \right) \tag{2-8}$$

where w is the strain energy density and s is distance along the arbitrary path, Γ, around the crack tip. T_i and u_i are the component of the traction vector and the displacement vector, respectively.

He also showed that J to be equal to the energy release rate for a crack in an elastic-plastic material, analogous to G for linear elastic material. J is more general version of the energy release rate and for the special case of a linear elastic material only, J is identical to G. The energy release rate is generally defined as the potential energy that is released from a structure when the crack grows in an elastic material. However, much of the strain energy absorbed by an elastic-plastic material is not recovered when the crack grows or the specimen is unloaded; a growing crack in an elastic-plastic material leaves a plastic wake. Thus the energy release rate concept has a somewhat different interpretation for elastic-plastic materials. Consequently, the energy release rate of J is useful for elastic-plastic materials when applying in appropriate manner.

2.1.3.4. Relationship among fracture parameters

As mentioned above, for linear elastic condition, the J-integral is identical to G, the energy release rate per unit crack extension. Therefore it is possible to infer “equivalent” K_{IC} values from J and CTOD by exploiting the relationships among three fracture toughness parameters for the linear elastic case.

Under plane strain linear elastic conditions,

$$J_{IC} = G_{IC} = \frac{(1-\upsilon^2)K^2{}_{IC}}{E} \tag{2-9}$$

The CTOD parameter, δ , also is related to J as follows:

$$\delta = \frac{G}{m\sigma_{ys}} = \frac{K^2{}_{IC}}{m\sigma_{ys}E} \tag{2-10}$$

where *m* is a dimensionless constant that depends on the stress state and material properties, $1 \leq m \leq 2$. By Eq. (2-9) and (2-10), the fracture mechanics analysis can be expressed in terms of any one of the three parameters based on the relationships shown below.

a) For small scale yielding, an equivalent K_{IC}, denoted as K_{JC}, can be computed as follow:

$$K_{JC} = \sqrt{\frac{J_{IC} \cdot E}{1-\nu^2}} \tag{2-11}$$

b) An approximate relationship between the J-integral and CTOD is given by Eq. (2-12).

$$J_{IC} = m \cdot \sigma_{ys} \cdot \delta_{IC} \tag{2-12}$$

c) By combining the above equations, the equivalent value

computed from CTOD data is given by Eq. (2-13).

$$K_{JC} = \sqrt{\frac{m \cdot \sigma_{ys} \cdot \delta_{IC} \cdot E}{1 - \nu^2}} \qquad (2\text{-}13)$$

Some studies [44-45] indicate that flow strength, σ_{flow}, should be used in place of yield strength in Eq. (2-12) and (2-13).

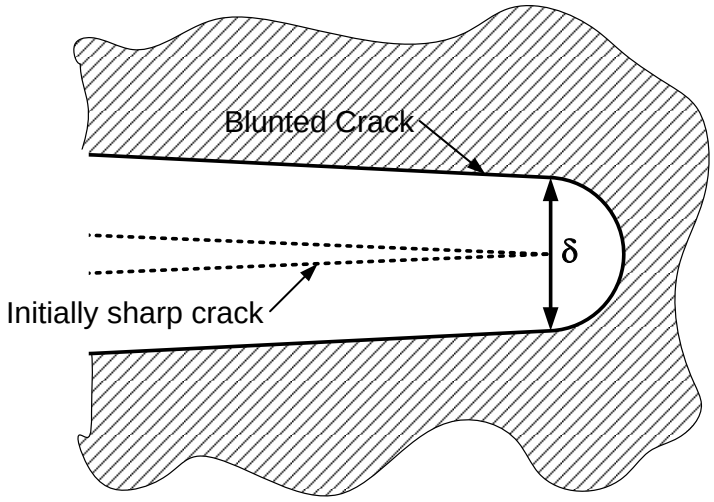

Fig. 2.6 Crack tip opening displacement (CTOD). An initially sharp crack blunts with plastic deformation, resulting in a finite displacement, δ, at the crack tip.

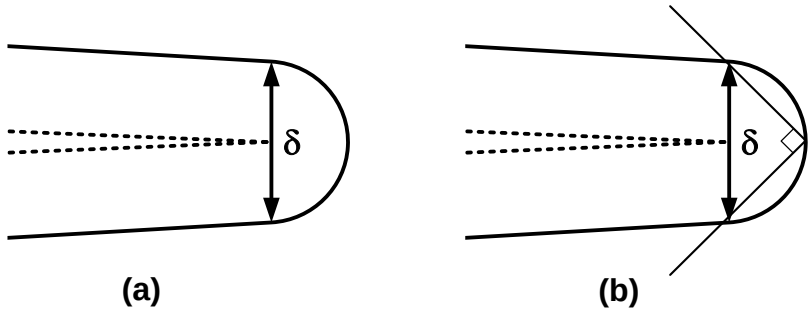

Fig. 2.7 Alternative definitions of CTOD: (a) displacement at the original crack tip and (b) displacement at the intersection of a 90^{o} vertex with the crack flanks.

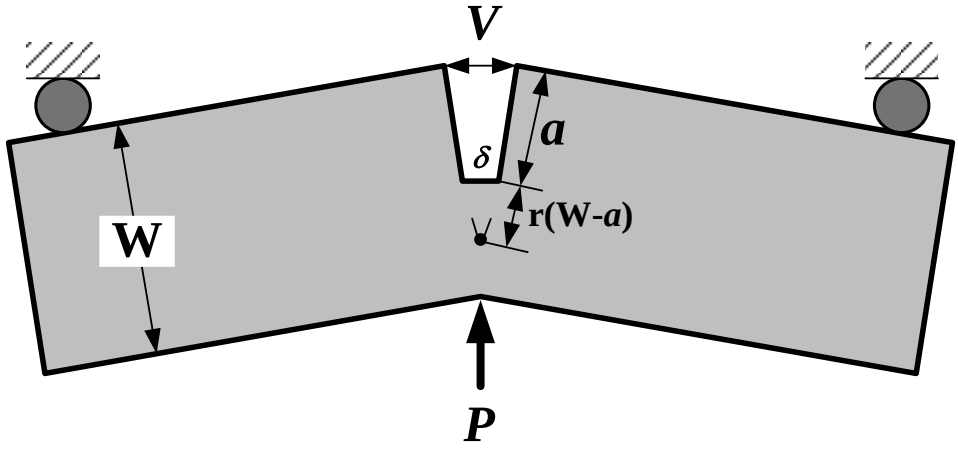

Fig. 2.8 The hinge model for estimating CTOD from three-point bend specimens [43]

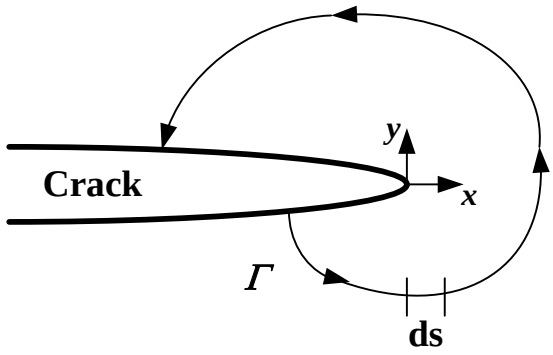

Fig. 2.9 Arbitrary contour around the tip of a crack

2.1.4. Measurement of fracture toughness

2.1.4.1. ASTM standard fracture toughness tests

There are several ASTM testing methods developed to measure the various critical stress intensity factors for materials that exhibit different types of fracture behavior and the corresponding service conditions.

1) K_{IC} [46]

Plane strain fracture toughness vales obtained at slow loading rates. Plane strain refers to conditions of maximum constraint, e.g., generally thick plates and deep cracks. Fracture is sudden, resulting in unstable brittle fracture with little or no deformation.

2) δ_c [47-49], J_c [50]

Elastic-plastic plane stress behavior during slow loading accompanied by plastic zone development, but not stable crack growth. Failure is by rapid unstable brittle fracture.

3) J_{IC} [51]

Critical value of the J-integral that describes the stress-strain field ahead of a crack is a measure of the fracture toughness at the onset of slow stable crack extension. Behavior is non-linear elastic plastic.

4) δ_u [47-49], J_u [50]

This quantity means elastic-plastic behavior during slow loading accompanied by slow stable ductile crack growth. This stable crack growth is either followed by brittle fracture or continued stable ductile crack growth until separation of the test specimen.

5) J_C, J_{IC}, J-R [51]

A new test method has been developed to cover all J-integral test results in one standard. Behavior would be elastic-plastic with or without stable crack extension.

6) K, J, CTOD *(δ)* [52]

This standard effectively replaces all of the previous test methods. A new common fracture test method, called the Standard Test Method [51], has been developed for materials where the type of behavior and thus the type of test needed also is not known before testing. A bend or compact specimen is tested and the P-δ_{CMOD} and P-δ_{LLD} records, where CMOD is the crack mouth opening displacement and LLD is the load line displacement, are analyzed as either of three fracture toughness values, depending on the test records.

7) K_{JC} [53]

This test method covers the determination of a reference temperature, T_o, that characterizes the fracture toughness of ferritic steels that experience onset of cleavage cracking at elastic, or elastic-plastic K_{IC} instabilities, or both [53]. This method treats the statistical effects of specimen size on K_{JC} in the transition range using the weakest link theory applied to a three-parameter Weibull distribution of fracture values [54]. Accordingly, it has advantages in dealing with the variability of test results.

2.1.4.2. Limitations and alternative approach

This chapter is devoted to a brief review of the estimation of fracture toughness (K_{IC}) by methods other than the standard fracture toughness test. These standard tests have significant limitations: 1) complex test procedures, 2) strict requirements for validating K_{IC}, primarily because of thickness effects, and 3) the effects of pre-existing defects. Consequently, K_{IC} values obtained in different works show large variations, and many researchers have tried to find alternative approaches that are easier and more convenient.

One such approach is to calculate the area under the stress-strain curve from a tension test [55], a value is simply known as *material toughness*. In general, fracture toughness can be defined as the strain energy absorbed by a material prior to fracture. The area under the stress-strain curve is a measure of fracture toughness in terms of the strain energy density, which is not a common variable in structural engineering analysis but may be used as a controlling parameter in classifying structural materials. Fig. 2.10 shows typical stress-strain curves characterizing the behavior of an initially crack-free material. A material of high strain-energy density usually has higher fracture toughness than a

material of low strain-energy density. However, when a notched tensile specimen of a ductile material is loaded in tension, the plastic flow is shifted upwards because a triaxial stress state is developed at the root of the notch. This means that a strain-energy density derived from the tensile curve is significantly affected by the presence of a notch in the specimen, and that the fracture toughness in terms of strain-energy density of crack-free materials does not apply to the fracture behavior of materials with cracks.

Nevertheless, attempts to estimate fracture toughness from tensile properties continue to evolve due to the simplicity and cost-effectiveness of the tension test. Many attempts have been made to estimate the plane-strain fracture toughness K_{IC} of ductile materials from other properties. Such modeling encounters several problems [33]:

1) Stress-strain distributions in the plastic zone ahead of the crack must be known or assumed. In this respect strain hardening is very important.
2) The proper fracture criterion must be chosen. Ductile rupture is strain controlled, i.e. the local strain must exceed a critical value. This is sometimes considered the fracture strain at the crack tip.

3) The critical strain must be reached or exceeded over a certain distance or volume. A reasonable assumption is that this distance is equal to the particle spacing. However, there is a complication: the critical strain depends strongly on the stress state, which varies significantly near the crack tip.
4) Calculation of K_{IC} is based on the assumption that unstable fracture occurs when the fracture criterion is satisfied. But actual determination of K_{IC} involves 2% crack extension which, if stable, can cause a significant increase in stress intensity.

In view of these problems, it is clear that the evaluation of fracture toughness is often very inaccurate. Even so, Hahn and Rosenfield [29] proposed a semi-empirical model using the relation between fracture toughness and tensile properties. They characterized the shear strain at the crack tip by a characteristic length l^*, the width of the plastic zone close to the crack tip under plane strain, which depends on the strain-hardening exponent. Also, they argued that the crack-tip fracture strain ε^*_f can be related to the true strain ε_f in a tensile test. In this way, the plane-strain fracture toughness K_{IC} is formulated in terms of tensile properties by combining the various descriptions and correlating the result with

existing measurements:

$$K_{IC} = \text{const.} \sqrt{E \cdot \sigma_{ys} \cdot n^2 \cdot \varepsilon_f} \qquad (2\text{-}14)$$

where E is Young's modulus, n is the strain-hardening exponent, and ε_f is the true strain at fracture of a smooth tensile specimen. This expression is accurate to within about 30% for eleven different aluminum, titanium, and steel alloys.

The model of Hahn and Rosenfield contains only macroscopic parameters. The influence of microstructure on fracture toughness is therefore only implicit, i.e. by its effect on these parameters. An obvious extension of the model is to incorporate the observed behavior of microvoid nucleation and coalescence. This can be done by specifying that the average strain over the distance d between particles must equal ε^*_f for fracture to occur. Several relationships among fracture toughness, particle spacing, and other material properties have been derived [28,56-58] that incorporate the influence of microstructure in different ways: as microvoid diameter [56], dispersoid spacing [57], grain size [28], area fraction of coarse voids [58], and the like.

Barsom [59] suggested determining fracture toughness by the mechanical properties near the crack tip. He assumed that the fracture strain near the tip of a crack is the same as in a plane-strain tension specimen. Using the relation between the crack-tip strain and the crack-tip opening displacement, the plane-strain fracture toughness is approximated by:

$$K_{IC} = A\sqrt{\sigma_{ys}}\ \ {\varepsilon_f}^2 \qquad (2\text{-}15)$$

where A is a material constant and ε_f is the plane-strain tensile ductility.

In addition, Teleshov et al. [60] and Oleinik et al. [61] proposed an empirical relation between the fracture toughness K_{IC} and mechanical properties such as tensile strength and percent elongation. From a hypothesis relating the fracture toughness and the thermo-activation energy of plastic deformation at the crack tip for BCC metals and alloys, Said and Tasgetiren [62] expressed the fracture toughness as a function of some mechanical properties and microstructure. Their model has the advantage of covering both quasi-static and dynamic loading. Baron [63] described the empirical relation among crack resistance, Brinell hardness, and yield strength of steels at various temperatures and deformation rates.

However, most alternative approaches have not been universally used to characterize the fracture behavior because the value of fracture toughness is intended to provide conservative, particularly fitness for service. Thus, although most codes and specifications were developed using principles of fracture mechanics, the specific fracture-toughness tests specified for material purchase or quality control are given in terms of auxiliary test specimens, such as the CVN (Charpy V-Notch) impact test specimen. Many correlations have been developed using a wide variety of test specimens. However, because the CVN test specimen has been the most widely used quality-control and specification specimen, correlations have been proposed primarily to relate the CVN test to K_{IC} results. Such correlations are summarized in Table 2.2 [64].

Hardness or instrumented indentation testing is commonly used to measure the mechanical performance of materials. In the 1950s, Palmquist [23] recognized that indentation-induced cracking observed on cermets was related to fracture toughness and developed a procedure to predict fracture toughness. Predicted values of fracture toughness for many brittle materials using empirical formulations from indentation theory can be found in the literature [65-69]

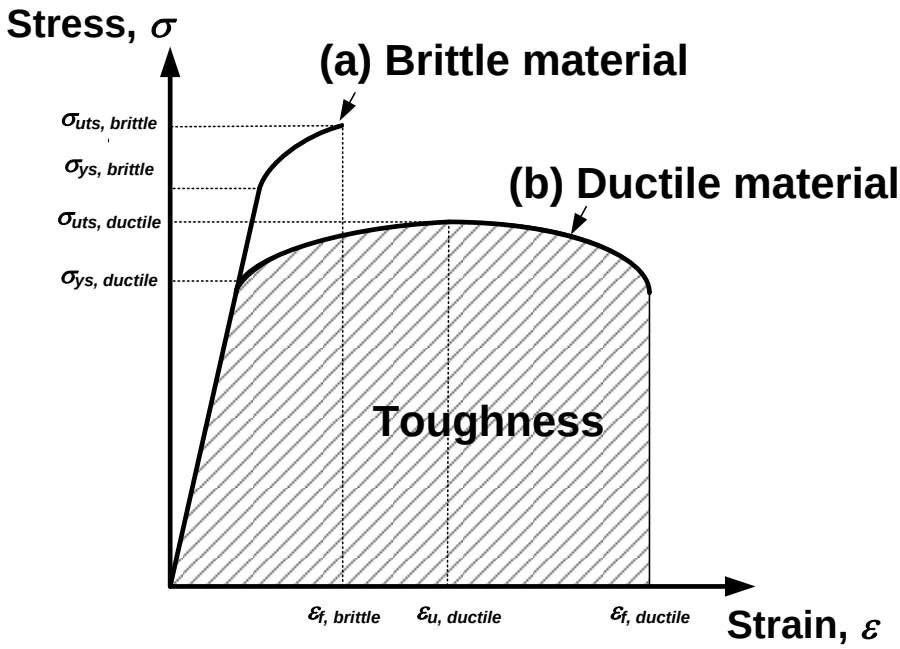

Fig. 2.10 Schematic of typical stress-stain curves

Table 2.2 Fracture Toughness-Charpy energy correlations [64]

Material	*Notch*	*Test*	*Temperature Range*	*Range of Charpy Results*	*Yield Strength Range (MPa)*	*Correlation*
A517D 4147 HY 130 4130 12 Ni-5Cr-3Mo 18 Ni-8Co-3Mo	V-Notch	Impact	Upper Shelf	31-121	760-1700	$\frac{K_{Ic}^2}{\sigma_{ys}} = 0.64\left(\frac{CVN}{\sigma_{ys}} - 0.01\right)$
High-Strength Steels	V-Notch	Impact	Upper Shelf	15-28.6	1610-1980	$\frac{K_{Ic}^2}{\sigma_{ys}} = 0.18\frac{CVN}{\sigma_{ys}} - 0.0011$
A517F A3202B ABS-C HY-130 18 Ni (250) Ni-Cr-Mo-V Cr-Mo-V Ni-Mo-V	V-Notch	Impact	Transition	4-82	270-1700	$\frac{K_{Ic}^2}{E} = 0.22(CVN)^{1.5}$
A533B A517F A542	V-Notch	Impact	Transition	7-68	410-480	$K_{Ic} = 14.6(CVN)^{0.5}$
En25 3% Ni-Cr-Mo-V	V-Notch	Impact	Transition	6-55	820-1420	$K_{Ic} = 18.2\frac{CVN^{0.5}}{A}$
HY60 Ti 3 Ti 6	V-Notch	Impact	Transition & Upper Shelf	5-125	400-560	$K_c = 15\frac{CVN^{0.543}}{A}$
ABS-C A305-B A517-F	V-Notch	Impact Slow Bend	Transition	2.7-61	250-345	$\frac{K_{Id}^2}{E} = 0.64CVN$ $\frac{K_{Ic}^2}{E} = 0.64CSB$
ABS-C A305-B A517-F A533-B	V-Notch	Impact	Transition	3-95	270-815	$K_{Id} = 15.5(CVN)^{0.375}$
A533-73 2.25% Cr-1Mo C-Mn-Nb-V 12MDV C4-03M	V-Notch	Impact	Transition	5-50	303-820	$K_{Id} = 19(CVN)^{0.5}$
ABS-C A302-B A517F	Precracked	Impact Slow Bend	Transition	2.7-61	250-345	$\frac{K_{Id}^2}{E} = 0.52PCI$ $\frac{K_{Ic}^2}{E} = 0.52PSB$
HY60	Precracked	Impact	Transition	16-40	400	$K_c = 25\frac{PCI^{0.5}}{A}$

2.2. Instrumented Indentation Technique

2.2.1. Introduction

Instrumented indentation technique has started from the conventional hardness test such as Vickers and Brinell hardness testing etc. Conventional hardness testing only measures hardness from residual imprint size, which means the resistance of the material to penetration. In the case of instrumented indention testing, however, the applied load and the depth of penetration of an indenter into the specimen are simultaneously recorded and used to indirectly determine the area of contact from indentation load-depth curve and hence the hardness of the test material [1-4]. The contact equations also allow the determination of the elastic modulus of the specimen [1-4]. Other properties such as the yield strength, tensile strength, strain hardening exponent [16, 17], fracture toughness [28, 30-32], and residual stress [18-22] can also be obtained in some circumstances.

The merits of instrumented indentation technique are 1) its simplicity, 2) it can be applied to microstructural constituent using micro or nanoindentation, 3) it is cost effective since small specimens are needed,

and 4) the tests are considered nondestructive in a macroscale, which on-site testing becomes available. Although it is difficult to make a comparison with the conventional mechanical test, however, specimen preparation is a slightly time consuming procedure since a polished surface is required so that uniform indentations are made on a reflective flat plane, which it is must in order to obtain consistent and reproducible results.

According to the applied load range, instrumented indentation test is classified into three categories: macro, micro, and nano. A macroindentation used mainly in the safety assessment of an in-service component due to its nondestructive feature. Micro or nanoindentation is now one of the most powerful tools for evaluating material properties and deformation behavior at small scales as thin films, MEMS, and bio-tissues.

Over the past decade, the standardizations with regard to instrumented indentation have become active discussion all over the world. The ISO 14577-1[70] as the most fundamental standard specifies not only the method of instrumented indentation test for hardness and material parameter, but the method of verification and calibration of testing machine. The part of ISO 14577-4[71]which describes a method for

testing coatings that is particularly suitable for testing in the micro/nano range applicable to thin coatings is also under discussion. In addition, a new ISO technical report, TR 29381:2008[101], has been established that describes three methods by which instrumented indentation tests can determine the tensile properties of metallic materials. Of three methods, the representative stress and strain method have been developed and proposed by our laboratory since 2003, including a procedure given for appendix for evaluating residual stress using an instrumented indentation tests.

2.2.2. Indentation tensile properties

The algorithm for evaluating tensile properties has four steps: step 0 — determine real contact area; step 1 — define representative stress and strain; step 2 — fit to constitutive equation; and step 3 — evaluate tensile properties. Details are as follows.

Fig. 2.11(b) shows a typical indentation load-depth curve obtainable during instrumented spherical indentations on steel. Unlike curves from sharp indentation (Fig. 2.11(a)) using pyramidal indenter, loading curves are quite linear due to the counterbalance of spherical geometry and

work-hardening in tested steel. Several depths are defined from this curve. The maximum indentation depth $h_{max}$is the total displacement of the material and the indenter at maximum load L_{max}, including elastic and plastic deformation. In unloading, elastic deformation is the indentation stiffness of the specimen and the indenter S. thus, the final depth h_f is the plastic deformation of the material.

A contact depth h_c^* at maximum indentation load can be evaluated by analyzing the unloading curve using the concepts of indenter geometry and elastic deflection [2]:

$$h^*_c = h_{max} - \omega\ (h_{max} - h_i) \qquad (2\text{-}22)$$

where h_i is the intercept indentation depth and the indenter shape parameter is 0.75 for a spherical indenter. The material pile-up around the indentation enlarges the contact radius (from the analysis of elastic deflection) by an extent that is determined by the work-hardening exponent n and the ratio of maximum indentation depth and indenter radius h_{max}/R [4]:

$$h^*_{pile} = h^*_c \cdot f\ (n, h_{max}\ /\mathrm{R}) \qquad (2\text{-}23)$$

where h^*_{pile} is the plastic pile-up depth.

The mean pressure p_m obtained by dividing the maximum load L_{max} by the contact area πa^2_c is well known to be about three times the representative stress σ_R for fully plastic deformation of steels [4]. In other words, the representative stress can be expressed as:

$$\sigma_R = \left(\frac{1}{\psi}\right) P_m = \left(\frac{1}{\psi}\right)\left(\frac{L_{max}}{\pi a_c{}^2}\right) \qquad (2\text{-}24)$$

where ψ is a plastic constraint factor, here taken as 3, and a_c is the contact area. On the basis of the deformation shape and strain distribution under a spherical indenter, Ahn and Kwon [16] proposed a new definition using the tangent function and a strain proportional constant, α:

$$\varepsilon_R = \left(\frac{\alpha}{\sqrt{1-(a_c/R)^2}}\right)\left(\frac{a_c}{R}\right) = \alpha \tan\gamma \qquad (2\text{-}25)$$

where α was determined as 0.14 by finite element analysis for various materials [72] , R is the indenter radius and is the half-angle between the

indenter and the material. The true stress and strain points obtained from the indentation test are then fitted to a constitutive equation by a simple power-law-type Hollmon equation:

$$\sigma = K \cdot \varepsilon^{n} \tag{2-26}$$

where *n* is the work-hardening exponent and the gradient of the curve, *K* is the strength coefficient, and are respectively the representative stress and strain values. This approach assumes that the flow curve of many metals in the uniform plastic deformation region can be expressed by Eq. (2-26). With most materials there is a gradual transition from elastic to plastic behavior, and the point at which plastic deformation begins is hard to define with precision. Although there are various criteria for the initiation of yielding, the yield strength obtained by an offset method is commonly used for design and specification purpose because it avoids the practical difficulties of measuring the elastic limit or proportional limit [73]. Thus, the yield strain can be determined as the intersection point of an elastic line whose slope is the elastic modulus 0.2% offset from the origin and a plastic curve of the constitutive equation. The uniform tensile strain should be same as the work-hardening exponent, by

the theory of instability in tension [73], and from this the indentation tensile strength can be determined. The indentation yield strengths and the indentation tensile strengths lie within 10% and 5% errors of those from uniaxial tensile tests, respectively [17, 74].

2.2.3. Residual Stress

Indentation hardness as analyzed from the indentation P-h curve changes with the material residual stress: indentation P-h curves are shifted with the direction and magnitude of residual stress within the tested material. However, the variations in the apparent indentation hardness with change in residual stress have been identified as an artifact of erroneous optical measurements of the indentation imprint [18, 19]: in a study of the influence of in-plane stress on indentation plasticity that investigated both the shape of the indentation curve and the contact impressions, the contact hardness was found to be invariant regardless of the elastically applied stress (residual stress) [18, 19]. The FEA results showed the important role of sink-in or pile-up deformations around the contact in the stressed state in producing the stress-insensitive contact hardness [20]. Therefore, the change in contact morphologies with

residual stress was modeled for constant maximum indentation depth assuming the independence of intrinsic hardness and residual stress [21].

The change in indentation deformation caused by the residual stress was identified in the indentation loading curve in Fig. 2.12. The applied load in the tensile-stressed state is lower than that in the stress-free state for the same maximum indentation depth [18, 19, 21]. In other words, the maximum indentation depth desired is reached at a smaller indentation load in a tensile-stressed state because a residual-stress-induced normal load acts as an additive load to the applied load. Therefore, the residual stress can be evaluated by analyzing the residual-stress-induced normal load.

The detailed changes in contact morphology can be seen in the schematic diagram in Fig. 2.13. The residual stress is relaxed from a tensile-stressed state to stress-free state while maintaining the constant maximum depth, h_{max}, as the stress relaxation pushes the indenter out from the surface. The pushing force appears as an increase in the applied load ($L_T \rightarrow L_0$) and the contact depth ($h_c^T \rightarrow h_c$), because the maximum depth is held constant. The indentation load and maximum depth for the tensile-stressed state (L_T, h_{max}) are equivalent to those in the relaxed state (L_0, h_{max}). Thus, the relationship between the two states can be expressed

as

$$L_0 = L_T + L_{res} \tag{2-27}$$

In the compressive stress state, the applied load and contact depth decrease by stress relaxation under the maximum-depth-controlled path. Furthermore, this decreasing portion of the applied load was the residual-stress-induced normal load, L_{res}. Therefore, the residual stress in a welded joint can be evaluated by dividing L_{res} by the contact area, A_C, regardless of the stress state [22]

$$\sigma_{res} = \alpha \frac{L_{res}}{A_c} \tag{2-28}$$

where α is a constant related to the stress directionality of biaxial residual stress. The biaxial stress state, in which $\sigma_y = k\sigma_x$, can be divided into a mean stress term and plastic-deformation-sensitive shear deviator term [22]

Biaxial stress *Mean stress* *Deviator stress*

$$\begin{pmatrix} \sigma^{x}_{res} & 0 & 0 \\ 0 & \sigma^{y}_{res} & 0 \\ 0 & 0 & 0 \end{pmatrix} = \begin{pmatrix} \frac{1+k}{3}\sigma^{x}_{res} & 0 & 0 \\ 0 & \frac{1+k}{3}\sigma^{x}_{res} & 0 \\ 0 & 0 & \frac{1+k}{3}\sigma^{x}_{res} \end{pmatrix} + \begin{pmatrix} \frac{2-k}{3}\sigma^{x}_{res} & 0 & 0 \\ 0 & \frac{2-k}{3}\sigma^{x}_{res} & 0 \\ 0 & 0 & -\frac{1+k}{3}\sigma^{x}_{res} \end{pmatrix} \quad (2\text{-}29)$$

The stress component parallel to the indentation axis in the deviator stress term directly affects the indenting plastic deformation. A residual-stress-induced normal load L_{res} can be defined from the selected deviator stress component as:

$$L_{res} = \frac{1+k}{3}\ \sigma_{res} A_c \quad (2\text{-}30)$$

Therefore, α in Eq. (2-28) can be taken as approximately 1.5 in the equi-biaxial stress state. In the instrumented indentation test, the contact area is determined by unloading curve analysis. By differentiation of the power-law-fitted unloading curve at maximum indentation depth, the contact depth and contact area can be calculated from the contact depth based on the geometry of the Vickers indenter as [2]:

$$A_c = 24.5{h_c}^2 \quad (2\text{-}31)$$

Thus, residual stress was calculated from the analyzed contact area in Eq. (2-30) and the measured load change L_{res} by the effect of residual stress in Eq. (2-27).

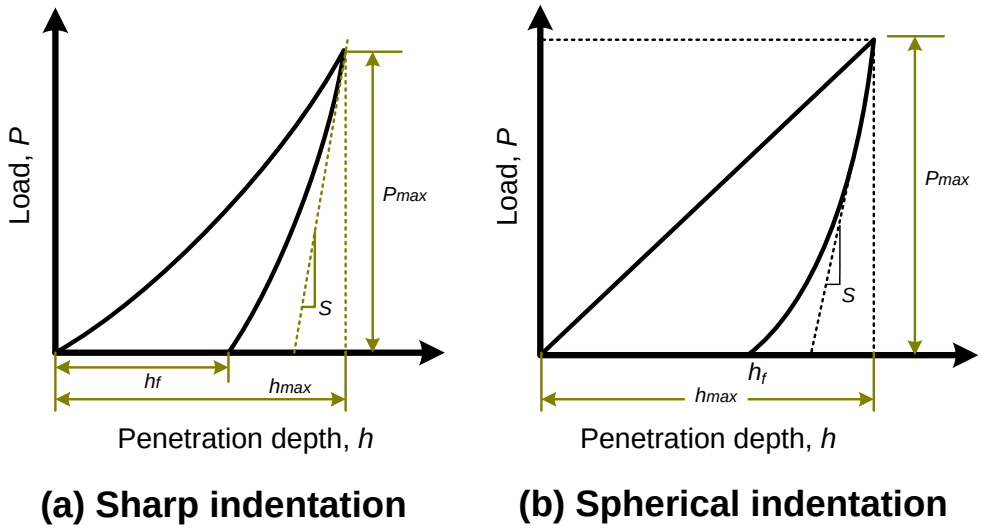

Fig. 2.11 Schematic diagram of typical load-depth curve obtainable during instrumented indentations

(a) Sharp indentation and (b) Spherical indentation

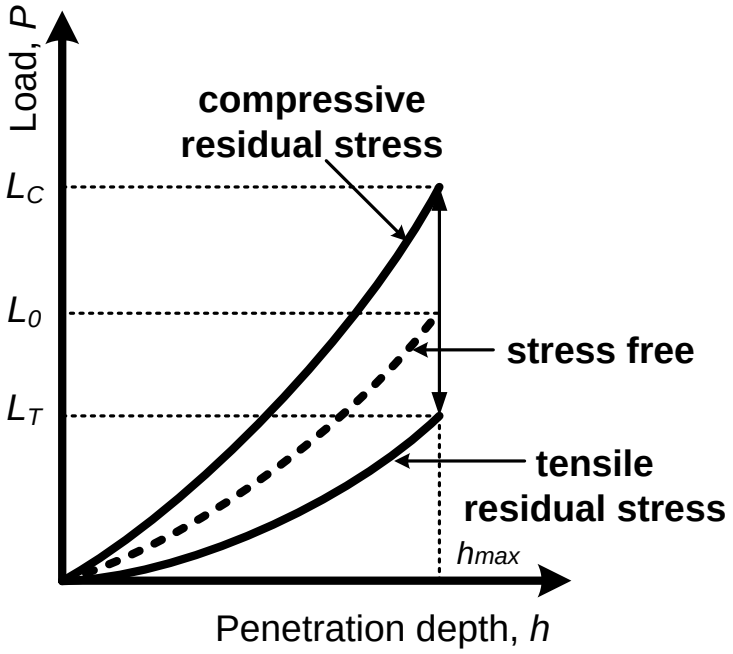

Fig. 2.12 Variation of indentation loading curves with changes in the stress state.

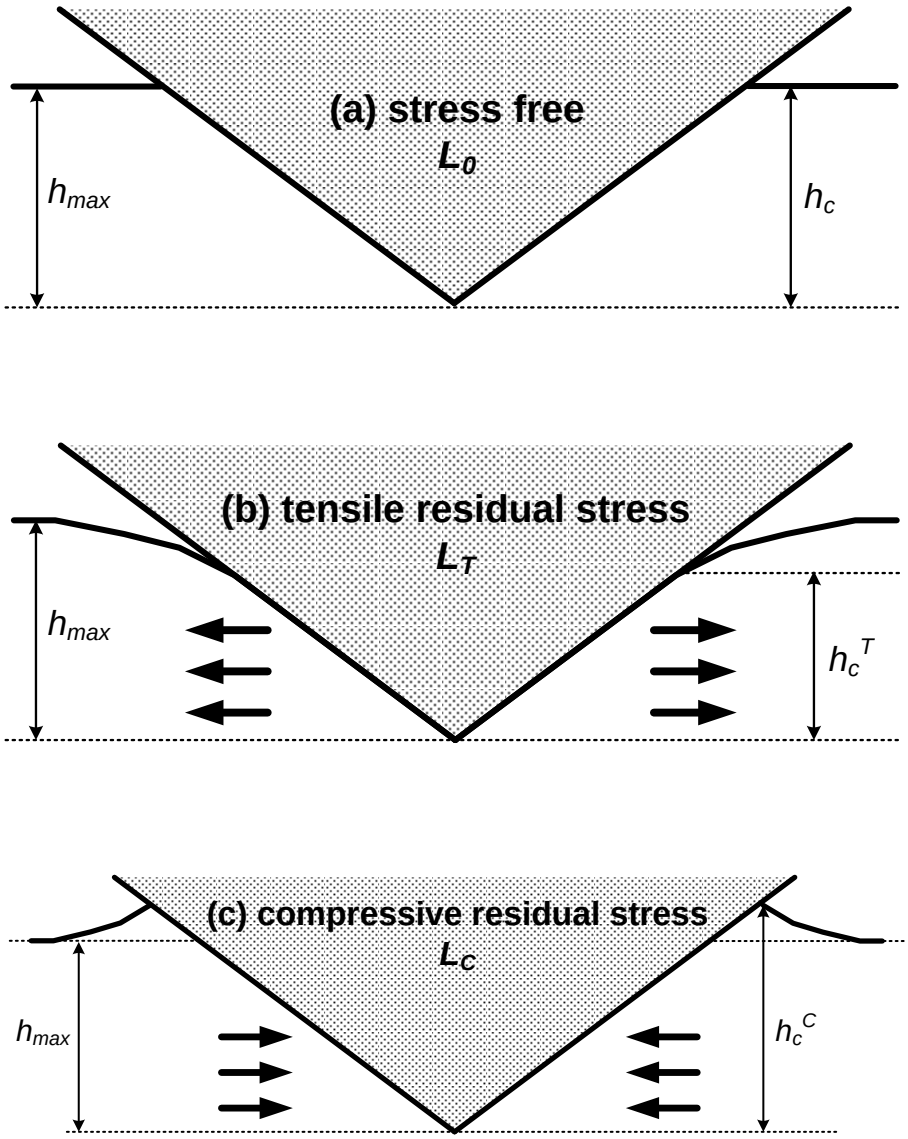

Fig. 2.13 Theoretical surface morphologies around the contact for (a) stress-free, (b) tensile stress, and (c) compressive stress states.

2.3. Indentation Fracture toughness

2.3.1. Introduction

Due to the simple test procedure and possibility of in-service test, instrumented indentation test is the one of the most attractive tool to measure mechanical properties of structures. Nevertheless, fracture toughness is one of the biggest barrier for indentation test. The biggest problem is that cracks or flaws does not occur during the test and since, only for ceramic materials and high hardness materials such as W-based tool steels, indentation cracking method that can make cracks during the test can determine the indentation fracture toughness. Thus, for metallic materials, many researchers has tried to developed alternative methods.

Most researchers [28-32,75] used spherical indenters. Since the technique for evaluating tensile properties using spherical indenters has been developed for a long time, a combination of mechanical parameters including tensile properties was first attempted. Then, in each indentation state, a specific point that could be related to the onset of cracks was determined, and fracture toughness was determined through criterion to that point. Recently, Kim et al. [76] proposed a model for evaluating

fracture toughness with a flat-ended cylindrical indenter. Based on the geometric similarity between the cylindrical indenter and the cracked round bar, the fracture toughness was calculated by determining the crack initiation point for the ductility and brittle fracture behavior, respectively.

2.3.2. Indentation cracking methods

Instrumented indentation can be used to evaluate the fracture toughness of materials and interfaces in a similar manner to that conventionally used in larger scale testing. During loading, tensile stresses are induced in the specimen material as the radius of the plastic zone increases. Upon unloading, additional stresses arise as the elastically strained material outside the plastic zone attempts to resume its original shape but is prevented from doing so by the permanent deformation associated with the plastic zone. There exists a large body of literature on the subject of indentation cracking with Vickers and other sharp indenters.

In general, there are various types of crack, and they are illustrated in Fig. 2-14 [102]. Radial cracks are vertical half-penny type cracks that occur on the surface of the specimen outside the plastic zone and at the corners of the residual impression at the indentation site. These radial

cracks are formed by a hoop stress and extend downward into the specimen but are usually quite shallow.

Lateral cracks are horizontal cracks that occur beneath the surface and are symmetric with the load axis. They are produced by a tensile stress and often extend to the surface, resulting in a surface ring that may lead to chipping of the surface of the specimen. Median cracks are vertical circular penny cracks that form beneath the surface along the axis of symmetry and have a direction aligned with the corners of the residual impression. Depending on the loading conditions, median cracks may extend upward and join with surface radial cracks, thus forming two half-penny cracks that intersect the surface as shown in Fig. 2-14(d). They arise due to the action of an outward stress. The exact sequence of initiation of these three types of cracks is sensitive to experimental conditions. However, it is generally observed that in soda-lime glass loaded with a Vickers indenter, median cracks initiate first. When the load is removed, the elastically strained material surrounding the median cracks cannot resume its former shape owing to the presence of the permanently deformed plastic material and this leads to a residual impression in the surface of the specimen.

Residual tensile stresses in the normal direction then produce a

horizontal lateral crack that may or may not curve upward and intersect the specimen surface. Upon reloading, the lateral cracks close and the median cracks reopen. For low values of indenter load, radial cracks also form during unloading (in other materials, radial cracks may form during loading). For large loads, upon unloading, the median cracks extend outward and upward and may join with the radial cracks to form a system of half-penny cracks, which are then referred to as median/radial cracks. In glass, the observed cracks at the corners of the residual impression on the specimen surface are usually fully formed median/radial cracks.

It is the radial and lateral cracks that are of particular importance, since their proximity to the surface has a significant influence on the fracture strength of the specimen. Fracture mechanics treatments of these types of cracks seek to provide a measure of fracture toughness based on the length of the radial surface cracks. Attention is usually given to the length of the radial cracks as measured from the corner of the indentation and then radials outward along the specimen surface as shown in Fig. 2.15. Palmqvist [23] stated that the crack length varied as a linear function of the indentation load. Lawn, Evans, and Marshall [27] formulated a different relationship, where they treated the fully formed median/radial crack and found the ratio P/c3/2 (where c is measured from the center of

contact to the end of the corner radial crack) is a constant, the value of which depends on the specimen material. Fracture toughness is found from:

$$K_c = \alpha \left(\frac{E}{H}\right)^{1/2} \left(\frac{P_{max}}{c^{3/2}}\right) \quad (2\text{-}32)$$

where a is an empirical calibration constant dependent on the geometry of the indenter. It was found that the value of 0.016 could give good correlation between the toughness values measured from the crack length and the ones obtained using more conventional methods [100]. An attractive feature of using this method in indentation is that both H and E can be determined directly from analyses of indentation force-depth data. Thus, provided one has a way to measure crack lengths, implementing the method is relatively straightforward.

2.3.3. Indentation fracture toughness model by spherical indenter

1) Critical strain model

Ju [31] was modified the critical strain model proposed by Hahn and Rosenfield [29] to evaluate the ductile fracture toughness using the

mechanical properties measured from the instrumented indentation tests. The modification of the critical strain model involved: 1) the use of fracture strain from the newly develop model, consisting the stress state, i.e. stress triaxiality, and deformation parameter which can be determined from indentation tests, instead of the critical strain at ahead of crack tip, and 2) the assumption of an empirical calibrated value for the characteristic length, l^*, as the function of the strain hardening exponent [29]. To determine the fracture strain, he adopted the void growth rate considered in a rigid-perfectly plastic material by Rice and Tracey [78]. Through its integrating, the fracture strain is given by:

$$\varepsilon_f = \ln\left(\frac{R_f}{R_i}\right)/0.32exp\left(1.5\frac{\sigma_m}{\sigma}\right) \qquad (2\text{-}33)$$

where R_f and R_i are the final and initial void radius, and σ_m and σ are the mean normal stress and the equivalent stress, respectively. He has shown experimentally that the ratio of void volume can be expressed by the reciprocal to the strain hardening exponent. Also ratio of stress is defined as the indentation parameter with regard to deformation. Thus, the critical fracture strain is expressed by:

$$\varepsilon_f = f\left(\frac{1}{n}\right) exp\left(1 - \frac{6A5^n}{\pi \cdot K}\right) \quad (2\text{-}34)$$

where A is the material yield parameter, *n* is strain hardening exponents, and K is the strength coefficient. From the relation between the characteristic length and strain hardening exponent [29], the modified critical strain model could be defined as:

$$K_{IC} = const. \sqrt{E \cdot \sigma_{ys} \cdot n^2 \cdot f\left(\frac{1}{n}\right) exp\left(1 - \frac{6A5^n}{\pi \cdot K}\right)} \quad (2\text{-}35)$$

where the constant is determined experimentally.

2) Continuum damage model

From Griffith theory [34], the relation of the fracture energy, wf and plane strain fracture toughness, KIC is expressed as following:

$$K_{IC} = \sqrt{2Ew_f} \quad (2\text{-}36)$$

where E is the elastic modulus. To estimate K_{IC} on the basis of Eq.(2-36) by using the indentation technique, w_f must be determined using only indentation parameters. Triaxiality ahead of the indenter tip is in the

range 2~3, and the degree of constraint in the deformed indentation region is similar to that ahead of the crack tip [30, 32, 79]. Hence the indentation energy per unit contact area to the characteristic point can be related to wf if there is a characteristic fracture initiation point during or over the indentation process. This energy, henceforth called the critical indentation energy, is calculated from the indentation load-depth curve:

$$2w_f = \lim_{h \to h^*} \int_0^h \frac{4P}{\pi d^2} dh \tag{2-37}$$

where P is the applied load, h is the indentation depth, d is the chordal diameter of the impression and h^* is the critical indentation depth corresponding to the characteristic fracture initiation point. $2w_f$ indicates the formation of two crack surfaces.

Since there are no distinguishing marks that can be used to identify fractures occurring during indentation, h^* in Eq. (2-37) cannot be measured by direct methods (optical microscope or SEM observation). Thus to determine h^*, continuum damage mechanics (CDM) was applied to the indentation process. CDM is used mainly to predict failure in structures loaded statically and dynamically. According to Lemaitre's

strain equivalence principle [80], damage variable D can be represented as following:

$$E_{eff} = E(1 - D) \tag{2-38}$$

where E_{eff} is the effective elastic modulus of the damaged material and E is the elastic modulus of the initial non-damaged material. E_{eff} decreases as *h* increases due to the increase in damage beneath the indenter [32]. In addition, E_{eff} is represented by a function comprised only of indentation parameters in Eq. (2-38)

From multiple loading-unloading, the values of E_{eff} for various indentation depths can be calculated from each unloading and E_{eff} vs. *h* may be plotted as in Fig. 2.16. If critical value of the elastic modulus is determined, h^* can be determined from the corresponding value of *h*. Since the indentation load is compressive in terms of the loading axis, the deformed region beneath the indenter experiences compressive stress. Hence, voids will be nucleated by localized shear due to compressive stress, and the void volume fraction, *f* will increase as *h* increases [81]. The D can be represented in terms of *f* as [80]:

$$D = \frac{\pi}{(1.3\pi)^{2/3}} f^{2/3} \tag{2-39}$$

From previous experimental and computational researches [82, 83], the void volume fraction, f of two types is proved; the values $f_C = 0.15$ (void volume fraction at onset of coalescence) and $f_F = 0.25$ (void volume fraction at initiation of stable crack growth). The concept of critical void volume fraction was adopted to determine the critical value of the elastic modulus. Critical CTOD are classified as δ_C, δ_U and δ_m, but ductile structural materials generally have δ_U and δ_m [47]. Since δ_U-type materials are brittle and have poor resistance to strain localization between voids compared to δ_m materials, they experience abrupt loss of load-carrying capacity soon after void coalescence begins. On the other hand, δ_m-type materials retain load-carrying capacity even after the onset of void coalescence, showing gradual loss of this capacity at the initiation of stable crack growth. With these phenomena in mind, f_C is used as the fracture criterion for δ_U-type materials and f_F is used for δ_m-type materials. The f_C and f_F can be converted into corresponding damage variables D_C and D_F through Eq. (2-39); then corresponding values of E_C and E_F are calculated by Eq. (2-38). Therefore, h^* is determined as the

corresponding h by using critical value of elastic modulus, $E^* = E_C$ for δ_m-type materials and $E^* = E_F$ for δ_U-type materials.

3) Critical stress / stain model (based on tensile properties)

Lee [84] and Jeon [75] proposed a critical stress model and a critical strain model that are applied differently according to the two different fracture behaviors of brittleness and ductility. The indentation critical stress model is based on an assumption that brittle fracture, i.e., cleavage fracture, takes place when the local tensile stress exceeds a critical value defined in terms of deformation flows during indentation. Thus, the critical stress model is applicable to brittle metallic materials with relative low fracture toughness (KJc < 100 MPa·m0.5) or the lower shelf region of the ductile-brittle transition curve. In contrast, the indentation critical strain is based on the modified critical strain model [31] and the relation between the J-integral and plastic deformation characteristics, such as strain energy density and plastic zone size. Thus, the critical strain model is applicable to ductile metallic materials with relative high fracture toughness (KJc > 250 MPa·m0.5) or the upper transition region of the ductile-brittle transition curve. Each fracture criterion was used to

determine the indentation fracture energy corresponding to the fracture energy required for crack extension.

The indentation critical stress model assumes that crack extension takes place when the local maximum tensile stress exceeds a critical value. To determine the critical stress value, they analyzed the indentation stress field based on contact mechanics. From contact mechanics, they divided the crack initiation into elastic and elastoplastic steps. In the first stage, they adapted Hertz's [85] elastic theory and maximum stress value in elastic stage represent as:

$$\sigma_r = \frac{(1-2\nu)}{2} \cdot p_m \qquad (2\text{-}40)$$

Inserting Eq. (2-40) into Tresca's yield criterion, results in Eq. (2-41),

$$p_m^y = C_1 \cdot \sigma_{ys} \qquad (2\text{-}41)$$

In this equation, C_1 is a constant that depends on the material and indenter geometry.

To analyze the elastic-plastic stress beneath a spherical indenter, they adapted Johnson's [86] model, expanding cavity model, which modification of Hill's spherical cavity model. A schematic diagram of the

stress field according to extended cavity model is shown in Fig. 2.17. They assumed that cracking only started when the plastic zone under the indenter was fully developed in the spherical indentation test. In addition, the fully developed plastic zone, from the Jones model, means the point where *c/a* (ratio of the plastic zone size and to the core radius in Fig. 2.17) does not increase any more, and the representative stress at that point is determined.

$$\frac{\Delta p_i}{\sigma_{ys}} = \frac{2}{3} + 2\ln\left(\frac{c}{a} - 1\right) \qquad (2\text{-}42)$$

where pi is the pressure inside the core and when c/a is constant this can be written as:

$$\Delta p_i = C_2 \cdot \sigma_{ys} \qquad (2\text{-}43)$$

Thus, we can determine the critical indentation stress by summing the mean pressure in the elastic indentation field and the core pressure in elastic-plastic indentation field from the surface to the indentation depth.

For ductile metallic materials, a large amount of plastic deformation occur before crack extension, so plastic deformation characteristics should be considered determining the critical point corresponding to crack extension in ductile metallic materials. Accordingly, we attempted to modify the critical strain model proposed by previous researchers [29]

on the basis of the relation between the J-integral and the plastic deformation characteristics such as the plastic zone size and the strain energy density, i.e., the tensile toughness. The J-integral has been used as a fracture parameter because of its path independence (the global and local energy release rates are equal), and it has frequently been used to describe the energy required for crack extension. A J-integral value that meets the size requirements can be converted to the fracture toughness KJc using Eq. (2-44) [40]:

$$K_{Jc} = \sqrt{\frac{J_{IC} \cdot E}{1-\nu^2}} \tag{2-44}$$

where E is the elastic modulus and v is the Poisson's ratio. The J-integral is actually accumulated in the form of plastic work in the specimen or structure during crack growth. Peel and Forsyth [87] assumed that the energy release per unit crack length is balanced by the amount of plastic work performed ahead of the crack tip. Thus, the plastic work performed at the crack tip is given by the following equation:

$$W_p = 2 \cdot r_c \cdot \left(\frac{dW}{dV} \right) \tag{2-45}$$

where W_p is the plastic work, r_c is the critical plastic zone radius at which stable crack extension begins ahead of the crack tip, and dW/dV is the strain energy density, i.e. tensile toughness. Assuming that $J_{IC} = W_p$ and substituting Eq. (2-45) into Eq. (2-44), we can rewrite Eq. (2-44) as follows:

$$K_{Jc} = \sqrt{\frac{2 \cdot E \cdot r_c \cdot \left(\frac{dW}{dV}\right)}{1-\nu^2}} \qquad (2\text{-}46)$$

The strain energy density is a tensile property that can be evaluated from the area under the tensile stress-strain curve. The area under the curve can be approximated by flow stress and fracture strain. The final equation can be expressed as following equation (2-47).

$$K_{Jc} = \sqrt{\frac{2 \cdot E \cdot r_c \cdot \sigma_R \cdot \varepsilon_f}{1-\nu^2}} \qquad (2\text{-}47).$$

where r_c is radius of plastic zone size.

From the above equation, they expressed the plastic zone size as a function of the resilience, and fracture strain was obtained by using the

experimental relationship with uniform strain.

2.3.4. Indentation fracture toughness model by flat punch indenter

The flat punch was introduced by paying attention to the geometric similarity between cracked round bar fracture specimen and flat punch and singularity at the tip end as shown in Fig. 2.18 and 2.19. Kim [88] considered the load-displacement curve obtained from a flat punch indenter as the load-displacement of the cracked round bar fracture test, and tried to determine the fracture toughness by setting an arbitrary crack initiation point in the load-displacement curve. He also proposed a ductile and brittle fracture model depending on the fracture behavior.

In ductile fracture model, the research results of cracked round bar fracture test is adapted for crack initiation point. Scibetta et al. [89] reported that the crack initiation point in the CRB fracture test occurred at the maximum load point in the load-displacement curve, and this point was calculated by3.285 times the yield strength of the material. Kim defined this point in his model on a normalized curve which is independent of the flat punch indenter radius to calculate the fracture toughness from the indention energy up to that point.

In the brittle fracture model, attention was also paid to the characteristics of the load-displacement curve of the material causing brittle fracture. In general, the material that causes brittle fracture usually cracks in the elastic region of the material, leading to fracture, so cracking occurs in a situation where plasticity does not occur in the load-displacement curve. Therefore, he used the 0.2% offset line, which is mainly used from an engineering point of view, to determine the initiation point of crack from the intersection of the offset line and the curve.

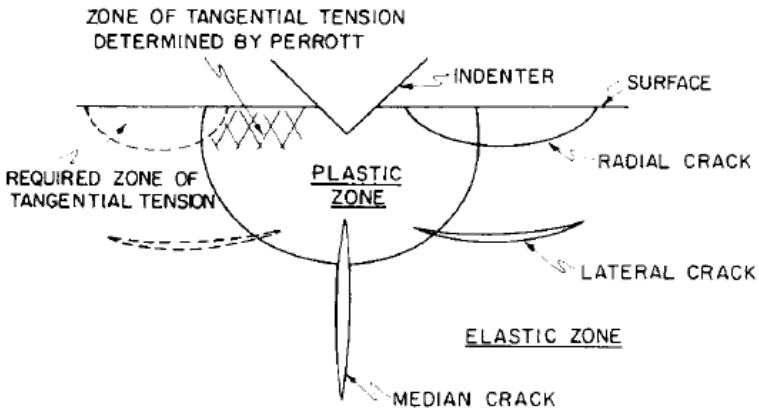

Fig. 2.14 Crack system for Vickers indenter: (a) radial cracks, (b) lateral cracks, (c) median cracks, and (d) half-penny cracks

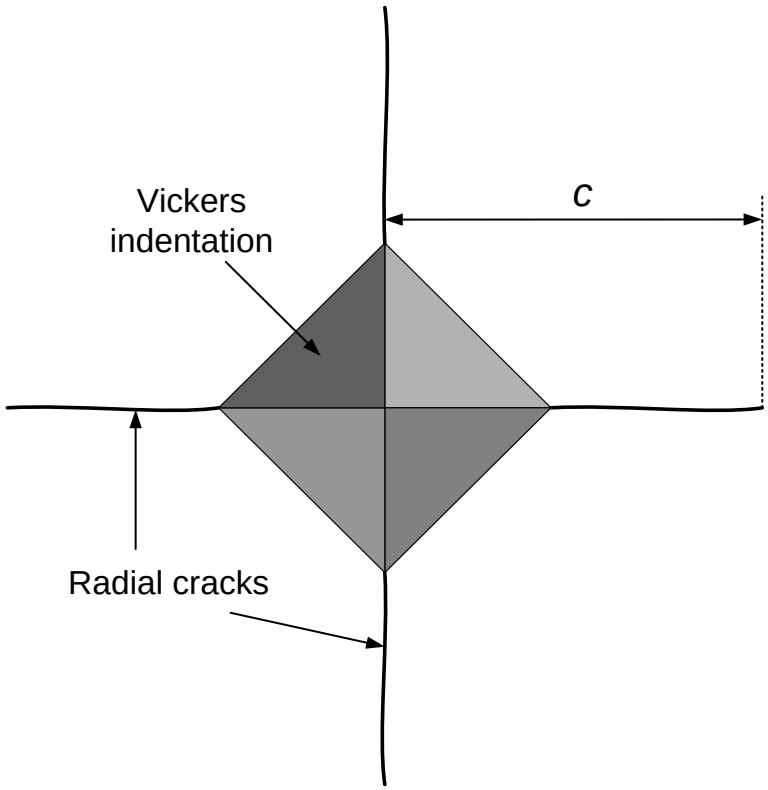

Fig. 2.15 Schematic of radial cracking by Vickers indentation

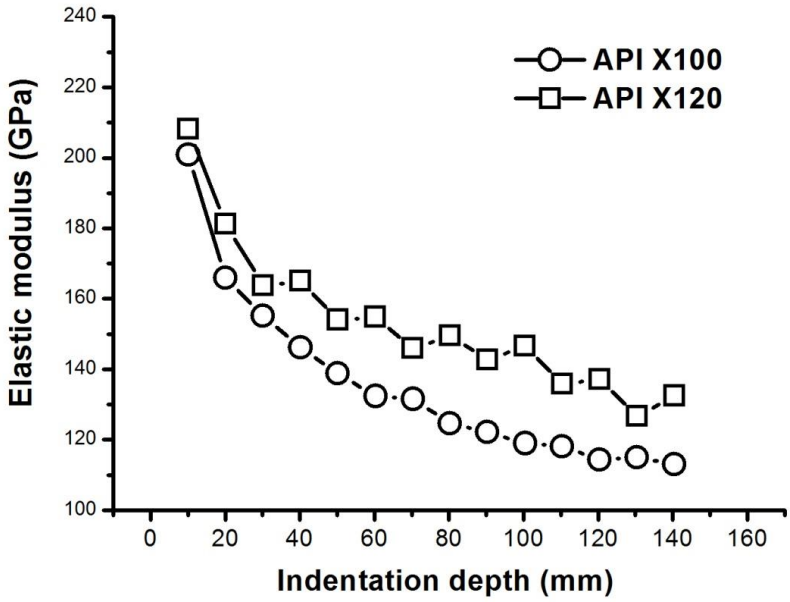

Fig. 2.16 Decreasing elastic modulus with indentation depth (API steels)

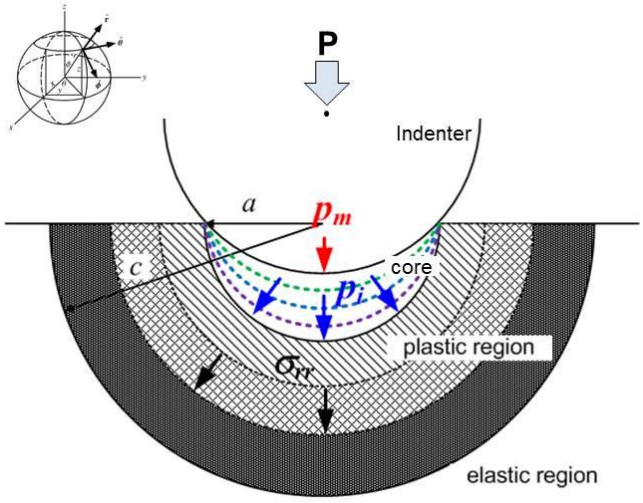

Fig. 2.17 Schematic diagram of expanding cavity model

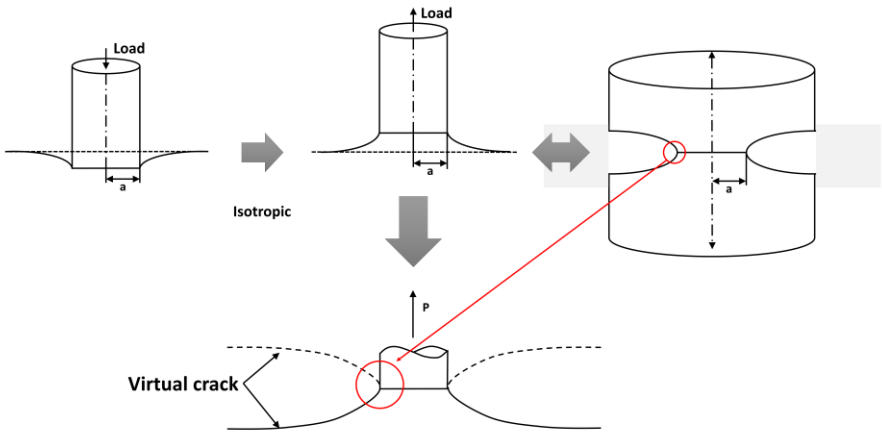

Fig. 2.18 The concept of flat indentation fracture toughness: Geometrical similarity between flat punch indentation and CRB fracture toughness test. [88]

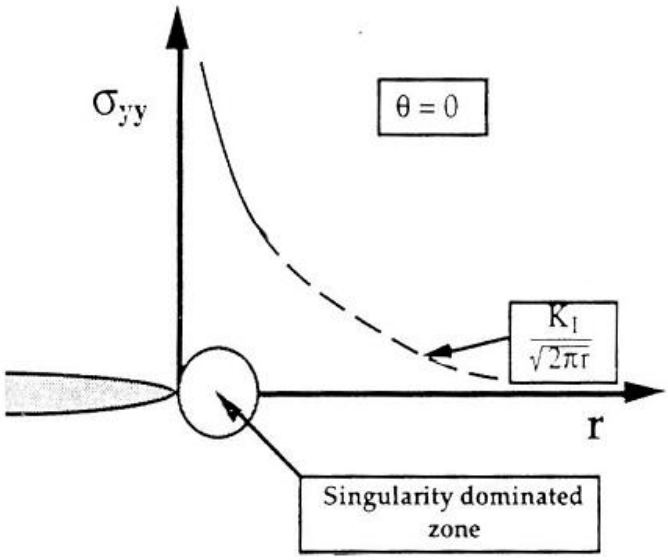

Fig. 2.19 Elastic stress field ahead of a crack tip

Chapter 3

THEORETICAL MODELING

Contents

3.1. Introduction

Indentation Fracture Toughness studies on metallic materials performed in the past have commonly determined a specific point in the indentation test as a critical point for calculating fracture toughness. This is because, in indentation experiments, cracks do not occur in metals, unlike ceramics such as glass or materials such as ultra-high hardness alloys. Lee et al. [32] assumed that the elastic modulus of the material changes during the indentation test from the perspective of the damage mechanics, but in reality, it is difficult to imagine the situation that the elastic modulus of the material changes by conducting a hardness test from the material itself. In other words, since crack-related information cannot be obtained during the instrumented indentation test for metals, it is inevitable to determine the virtual crack initiation point through a specific stress state or cracking concept. Therefore, in previous indentation fracture studies, the fracture toughness had to be expressed as a combination of mechanical parameters that can be obtained from indentation tests, or an empirical relationship in limited materials was used.

In this study, we tried to predict the fracture toughness by adopting a flat

punch indenter, because the stress state that can be obtained when using a flat punch indenter can be more similar to the stress state in front of a crack than using a spherical indenter. In particular, if we use a flat punch indenter, load-indentation depth curve can be expressed as normalized curve which is independent of the indenter radius; the load is converted to P_m and the indentation depth is converted to h/r as shown in Fig. 3.1. When using normalized curve that can be obtained regardless of the indenter radius, there is an advantage that the indenter size can be changed and applied according to experimental conditions. Above all, however, it is attractive in that it is possible to obtain a load-indentation depth curve of a larger radius sized indentation test even experimenting with a small indenter. Thus, from this the mention above, considering the geometric similarity with the cracked round bar fracture specimen mentioned in Kim's model [76], even if we obtain the load-displacement curve obtained from a small flat cylinder test with a radius of 250 μm, it is possible to obtain the fracture toughness value by converting to a load-displacement curve of radius of cracked round bar fracture specimen size equivalent to 1T thickness which is mainly used in general fracture tests..

In this study, two different crack initiation points were proposed

according to the fracture behavior. In the duck tile model, we tried to find a state similar to the crack initiation point in the cracked round bar fracture test in the flat indentation test. In the brittle fracture model, the stress intensity factor obtained in the flat punch indentation test was determined from the conditions satisfying the small scale yielding.

3.2. Ductile fracture model

According to previous researches on fracture toughness testing with circumferentially cracked round bar specimen, they reported that crack initiation occurs at maximum load in load displacement curve as shown in Fig 3.2 [89, 90]. Since the load is a function of the reduction of the ligament size due to crack blunting, necking or crack growth and the increase of the average axial stress due to higher constraint or strain hardening, the load drop can be occurred like as the necking point in tensile testing and the maximum load can be crack initiation point if we assume the load drop is only due to crack growth. And Scibetta et al. [89] suggested that the maximum load can be evaluated by the plastic limit load. Limit load is defined as load-bearing capacity in perfect plastic behavior of materials and a function of yield strength of materials and

geometrical constant. But in case of real materials, strain hardening is occurred so that the load calculated from theoretical limit load equation is not an end load point but a specific point. This point is matched well with crack initiation point in Scibetta′s study.

The limit load equation of circumferentially cracked round bar geometry is reported as [91]:

$$P_L = 2.845 \cdot \sigma_Y \cdot \pi r^2 \qquad (3\text{-}1)$$

for deeply cracked condition, where σ_Y is yield strength or flow strength of materials and r is ligament radius. The constant of 2.845 is derived from Tresca yield criterion so 3.285 can be also used by applying Von Mises yield criterion. In flat punch indentation, because indenter radius is very small compared to specimen size, virtual crack length per specimen size is almost 1, that is, very deep cracked condition, this equation can be applied. However, Eq. (3-1) is an empirical formula derived from limited materials, and there is different relation between the actual fracture toughness point and yield strength. Instead, Scibetta et al. [89,90] describe the state of the ligament at ahead of the crack as the state of the

plastic zone in front of the crack. They reported that when the cracked round bar fracture specimen is loaded, a plastic zone occurs in front of the crack, which grows at both ends of the crack, gradually expands and meets, and eventually all areas of the ligament are completely change into the plastic zone. They insisted the cracks propagate when the plastic zone grow up and reach that state, and this can be agreed well considering the state when shape of the rod type specimen is applied the destruction of the material starting like a necking in tensile test.

This perspective is also applied to the flat punch indentation test. When the flat punch indentation test is performed, a plastic zone is also generated beneath the indenter as shown in Fig. 3.3. Therefore, from the flat punch fracture toughness model [78] based on the similarity with cracked round bar, it is assumed that the flat punch indenter is a ligament of the cracked round bar fracture specimen, and the crack initiation point can be determined when the plastic zone occurring beneath the indenter is fully developed.

In determining the point where the plastic zone was fully developed, Lu et al. [92] reported that it can be inferred from the load displacement curve of a flat punch indenter. Fig. 3.4 is a typical load-depth curve of flat punch indentation. As shown in the Fig. 3.4, the load-depth curve appears

as a stress-strain curve, which is divided into three stages; firstly a linear stage at the beginning of press-fitting, an elastic-plastic stage where the slope of the curve changes, and a plastic deformation stage where a linear gradient occurs again [93]. Lu et al. [92], in their simulation studies, reported a fully developed zone formed at the beginning of this 3rd stage. Therefore, we determined the end of the elastoplastic stage (2nd stage) as the starting point of the deformation region (3rd stage) as the starting point of the crack. Lu et al. mentioned that the increase in load occurring in the 3rd stage arises from the friction force between the indenter and the specimen, which increases linearly with the indentation depth. Therefore, frictional component obtained from slope of 3rd stage in the raw load-displacement curve (when indenter radius is 250um) and then, the frictionless curve as shown in Fig. 3.5 obtained by subtracting the frictional force can be obtained and finally the indentation depth corresponding to the point when the plastic zone is fully developed.

3.3. Brittle fracture model

In contrast with ductile fracture mode, which shows stable crack extension, Brittle fracture mode shows that crack initiation and fracture is

occurred at the same time. Thus, crack initiation point is clear in load displacement curve of fracture toughness testing and estimating crack initiation is unconcerned in brittle fracture mode. In previous flat punch brittle fracture model, the crack initiation point was determined intuitionally using a 0.2% offset line [73]. In this study, instead of an engineering approach, we wanted to incorporate the content of fracture mechanics. Brittle fracture occurs when the energy that advances the crack exceeds a certain critical point, and this analysis is well explained in linear elastic fracture mechanics. Since plasticity is not considered in the linear elastic fracture mechanics, a condition to minimize the plastic strain energy as a validity to apply it is proposed. With this in mind, we applied the condition that the plastic strain energy is minimum, that is, the small scale yielding condition to the flat punch indentation test. Scibetta [94] express the size of a plastic zone to which linear elastic fracture mechanics is applied as follows:

$$r_p = \frac{1}{6\pi} \cdot \frac{K^2}{\sigma_0^2} \tag{3-2}$$

Where r_p is plastic zone size, K is stress intensity factor and σ_0 is yield stress of material. In Equation (3-2), from the small scale yielding

condition, the plastic zone size of cracked round bar is 1/25 of the ligament, and so if we use a flat punch with a radius of 250um, the plastic zone has a size of 10um. Then, *K* value can be calculated and the stress intensity factor equation in indentation test derived from study of Xie [95] and Sneddon [96] is expresses as :

$$K = \frac{P}{2r\sqrt{\pi r}} \qquad (3\text{-}3)$$

where *r* is the radius of indenter. Finally, we can find the load corresponding to *K* from the load-displacement curve of the flat punch indentation test and determine the fracture toughness from the indentation depth reaching that load.

3.4. Size adjustment

Fracture toughness is varied with specimen thickness and in ASTM E1921 [53], they recommend using 1 inch thickness specimen or converting fracture toughness value to that for 1 inch thickness fracture toughness specimen as shown in Fig. 3.6 instead of specimen size

requirement for plane strain condition. From this point, we simply adjust indenter size corresponding 1 inch thickness for standard fracture toughness specimen. Since the thickness of general fracture toughness specimen means crack front length, in case of circumferentially cracked round bar specimen, crack front length is circumference of ligament as shown in Fig. 3.7 and the indenter size corresponding 1 inch thickness is about 4 mm radius of flat punch indenter. Therefore, we can obtain the fracture toughness value corresponding to the 1T thickness fracture toughness test through the crack initiation depth obtained in the brittle and ductile models in the load-displacement curve with a 4mm radius.

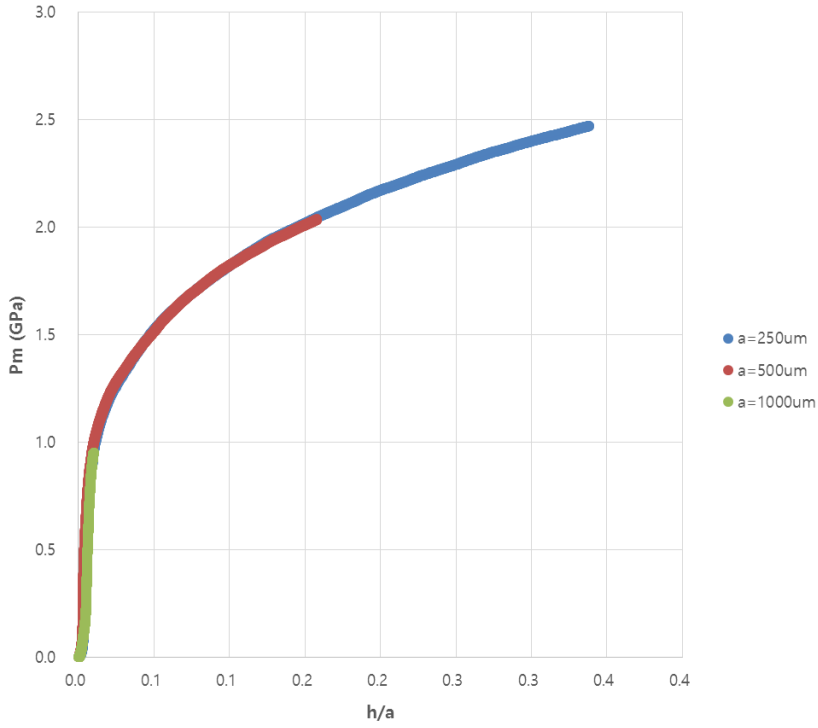

Fig. 3.1 Normalization of indentation load-depth curves using flat punch indenters of various indenter radius

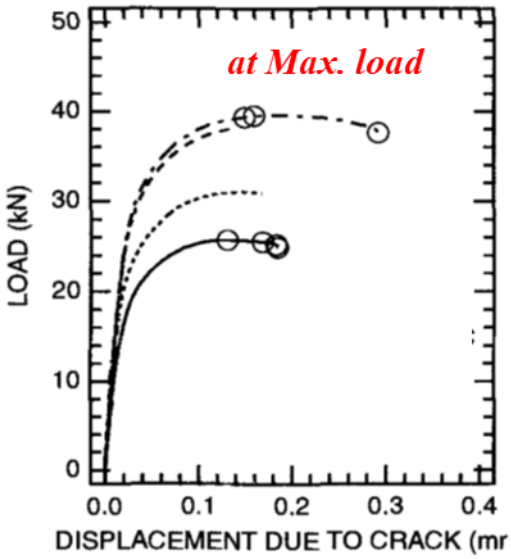

Fig. 3.2 Load displacement curves of circumferentially cracked round bar specimen with ductile fracture [89]

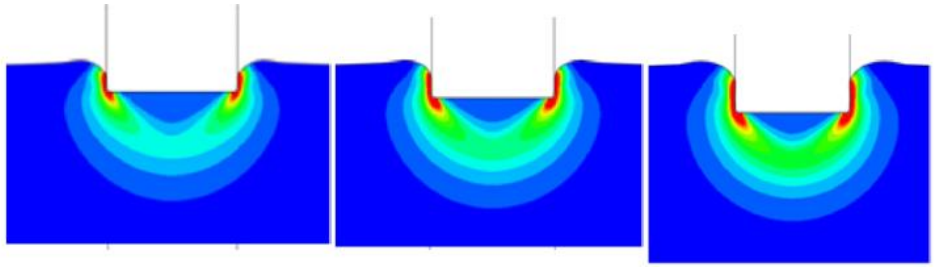

Fig. 3.3 Contours of equivalent plastic strain showing the development of plastic zone under a flat punch indenter

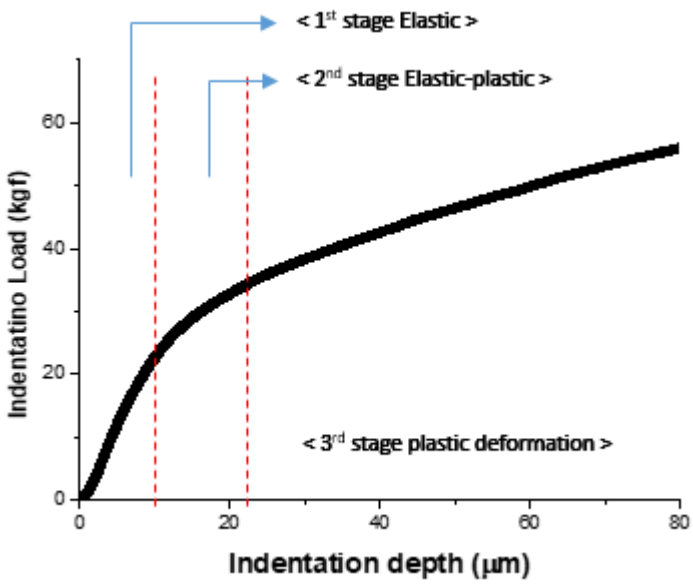

Fig. 3.4 Typical load-depth curve of flat punch indenter. The curve is divided into 3 stages. [93]

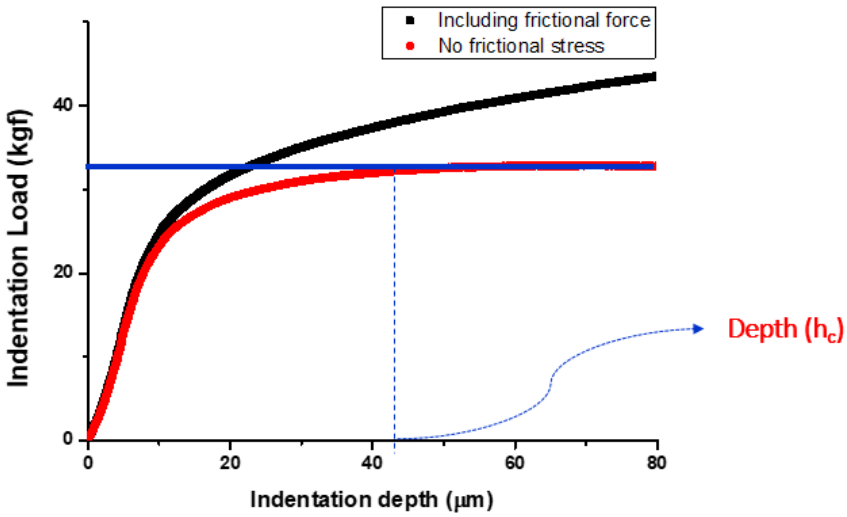

Fig. 3.5 Frictionless curve of flat punch indentation

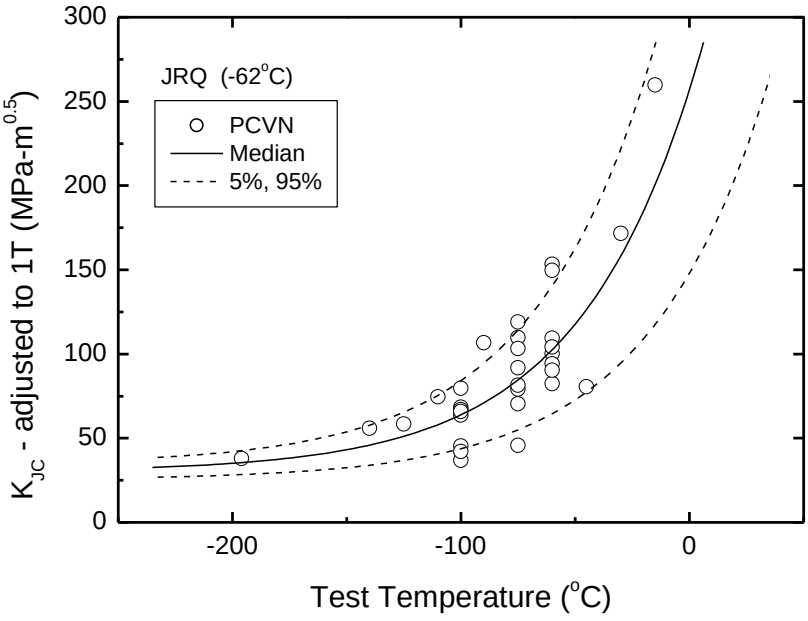

Fig. 3.6 Typical K_{JC} data adjusted to 1T (inch) thickness with temperature

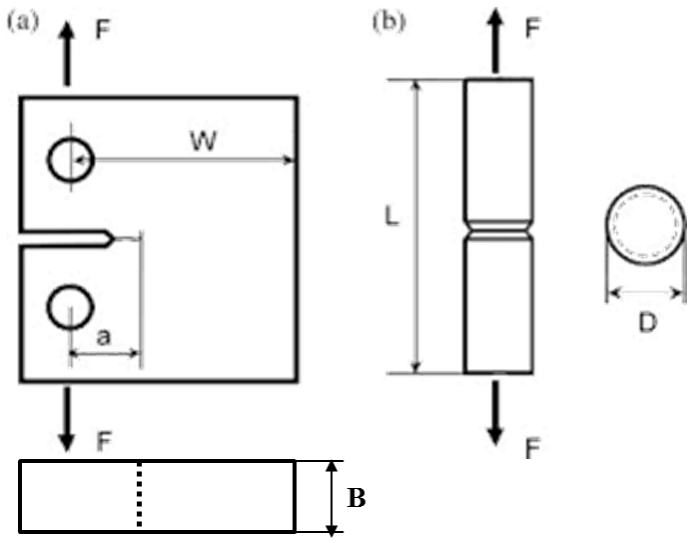

Fig. 3.7 Geometrical relationship between crack front length and specimen geometry

Chapter 4

Experimental verification

Contents

4.1. Materials and methods

To verify proposed indentation fracture toughness models, various kinds of metallic materials that evaluating fracture toughness is often required at the industrial fields are selected for flat punch indentation testing and conventional mechanical testing. The list and mechanical properties of selected materials are shown in Table 4.1.

Uniaxial tensile tests were carried out according to ASTM E8:09 [97] at room temperature. Test specimens used 6 mm diameter smooth round test specimens shown in Fig. 4.1, which is the small-size specimen proportional to the full-size one and the gage length was 25 mm. The tensile tests were performed by INSTRON 5582, material testing machine and the cross-head speed is 1 mm/min. To get reliable average values for the tensile properties, a minimum number of five tensile tests have been carried out.

Flat punch indentation tests were performed with the AIS 3000 portable indentation system in Fig. 4.2 (Frontics Inc., South Korea). This indentation equipment measured the real-time indentation load and depth through a 300 kgf load cell and a linear variable displacement transducer and its resolution is 0.002 kgf and 0.1 μm, respectively. The indenter was

a tungsten carbide cylindrical punch of 0.25 μm radius. Under displacement-controlled conditions at 0.3 mm/min indentation speed, the maximum indentation depth was 100 mm. At least three sets of indentation data were obtained from indentation tests for each material, and the average value was used in analyzing the fracture toughness. Indentation specimen was 30 x 30 x 10 mm and surfaces were finally polished with 1 μm Al_2O_3 powder.

The fracture toughness tests were performed using two different methods according to ASTM E1820 [52]: the basic procedure and the resistance curve procedure. The basic method was used to divide the material which is not occurred the significant stable crack growth prior to fracture instability. That is, the value of fracture toughness of brittle materials, J_C, was measured from the basic method. The resistance curve method was used to measure the fracture toughness, J_{IC}, near the onset of ductile crack extension, i.e. stable crack growth. A J-R curve was obtained from the single specimen unloading compliance method, which is illustrated in Fig. 4.4. The crack length is computed at regular intervals during the test by partially unloading the specimen and measuring the compliance.

The configuration of the SENB (single edge notched bending) specimens is shown in Fig. 4.5. All test specimens have an orientation corresponding to loading in the longitudinal direction and crack propagation in the transverse direction from rolled plate. Also, an orientation of specimen extracted from disk and hollow is L-R, i.e. loading in the longitudinal direction and crack propagation in the radial direction (Fig. 4.6)

Straight fatigue pre-cracks were made on the specimens in front of the side-notch to make the ratio of total crack length to the specimen width (a/W) valued between 0.5 and 0.7, which is because the unloading compliance technique is less sensitive for a/W < 0.5. The maximum load for the fatigue pre-cracking was calculated from:

$$P_m = \frac{0.5B\, b_0^2 \sigma_R}{S} \qquad (4\text{-}1)$$

where σ_R is the flow stress and is typically the average of the yield strength and ultimate tensile strength. After the pre-cracking, side grooves are machined into the sides of each specimen to maintain a straight crack front during a J-R curve test and the total thickness

reduction is 0.2*B*.

INSTRON 8503 was used as the equipment for fracture toughness test as shown in Fig. 4.7. The values of fracture toughness for each material were measured from three times tests at least and the average values were used as the representative fracture toughness. Tested materials are heated to measure the length of original crack, i.e. the length of fatigue pre-crack, and final physical crack length, i.e. the extended length after testing at about 300^{o}C for 30 min. The measuring instrumented was the stereographic microscopes and each crack length was measured at nine equally spaced points centered about the specimen centerline as shown in Fig. 4.8. The values of provisional J_{IC} are determined from the J-R curves shown in Fig. 4.9 and their validity check were also performed according to the data requirement in ASTM E1820 [52].

4.2. Results

Determination of fracture toughness using proposed indentation fracture toughness models is identical with standard fracture toughness testing, applying fracture mechanics as it is, because we modeled flat punch indentation as virtual fracture toughness testing with circumferentially

crack round bar specimen. Calculation of J is as follows [52]:

$$J_{IC} = J_e + J_p = \frac{(1-\nu^2)K_I^2}{E} + \eta_{pl}\frac{A_{pl}}{\pi r^2} \tag{4-2}$$

where K_I is stress intensity factor and is calculated using Eq. (3-3), E is elastic modulus, ν is poisson′s ratio, A_{pl} is area under load depth curve until determined crack initiation point, r is indenter radius as ligament radius, and η_{pl} is a factor for specimen geometry and crack size and 0.775 for circumferentially cracked round bar geometry. J_{IC} is converted to K_{JC} by

$$K_{JC} = \sqrt{\frac{J_{IC} \cdot E}{(1-\upsilon^2)}} \tag{4-3}$$

The values of fracture toughness obtained from Eq. (4-3) are illustrated in Fig. 4.10 and they are compared with those from *J*-tests.

The values of fracture toughness for ductile fracture model show about 20% deviation between both results in Fig. 4.10(a). It turns out that with

most materials the values of fracture toughness obtained from indentation are underestimated in comparison with them from fracture tests. If we take into account the universal deviation of fracture toughness in the upper shelf region, Fig. 4.10(a) shows mostly good agreement. In the case of SA516, although the indentation results is largely errored, it is acceptable in the conservative point of view. And, as shown in Fig. 4.11, the normalized curve and stress-strain curve from tensile test is not matched well in these cases. It may be the reason of poor results that indentation fracture toughness model has limitations and it needs further study.

The results from brittle fracture model in Fig. 4.10(b) are also approximately 20% deviation between the indentation and fracture tests over all except SKH51 which shows slightly larger error than others. This is expected because the fracture toughness value of SKH51 from J test is somewhat low contrary to expectations. Fracture toughness in brittle region has large scatter by its statistical nature and difference of microstructure. In this study, we did not consider material′s microstructural aspects and manufacturing direction which also affected to fracture toughness results, so it seems to cause the large error of final

results.

Table 4.1 List and mechanical properties for tested materials

		Tensile properties			Fracture toughness	
		E	YS	n	K_{JC} (avg.)	Stdev.
		GPa	MPa		$MPa\sqrt{m}$	
Carbon Steels & Alloy Steels	S20C	201.6	266.3	0.248	278.8	4.2
	SCM21	202.2	266.2	0.223	343.7	12.0
	SS400	188.2	308.6	0.237	310.2	0.1
	API X65	178.2	442.9	0.168	291.8	8.0
	A36	184.9	296.6	0.258	447.0	5.7
	SA516	202.0	292.4	0.226	499.5	18.2
	SA508Gr.1a	213.6	364.2	0.245	501.7	14.3
	SA508 Gr.3	214.9	470.2	0.212	340.0	15.5
	CA6NM	184.7	686.0	0.221	221.2	16.4
Tool Steels	SKD61	217.3	370.0	0.241	360.6	6.8
	SKS3	202.5	426.1	0.218	118.2	5.8
	SKH51	214.9	296.7	0.216	59.7	4.4
	SKD11	209.2	362.0	0.242	98.3	6.8
	SUJ2	174.7	356.3	0.239	113.8	13.0
Stainless steels	SUS304	171.0	234.1	0.358	349.2	17.1
	SUS304L	188.9	296.5	0.381	389.2	11.0
	SUS347	182.2	244.9	0.369	366.7	6.4
	SUS321	179.1	252.4	0.373	336.9	2.7

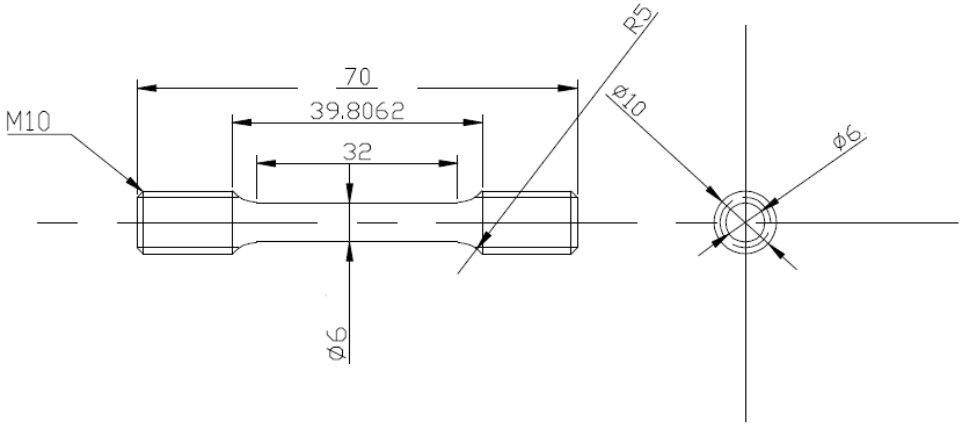

Fig. 4.1 Tensile specimen configuration according to specifications

ASTM E8:09

Fig. 4.2. AIS 3000 system for indentation.

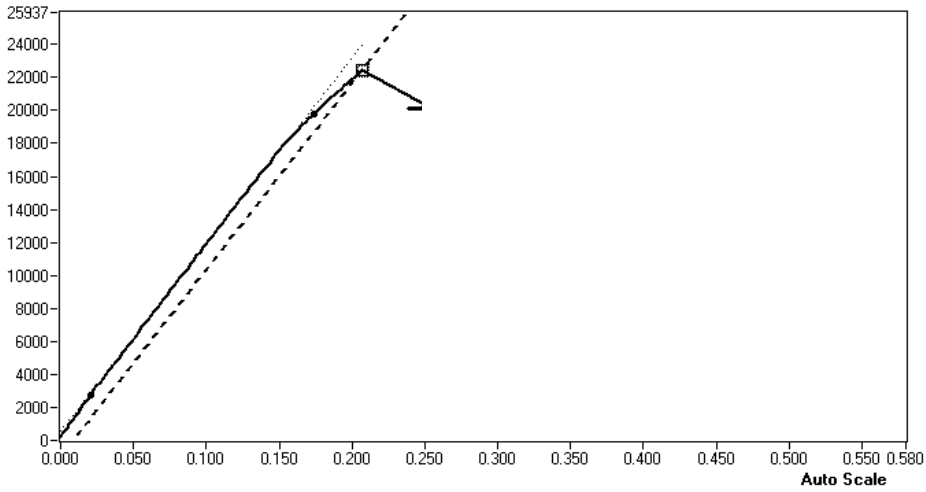

Fig. 4.3 Load and displacement curve measured from the basic method

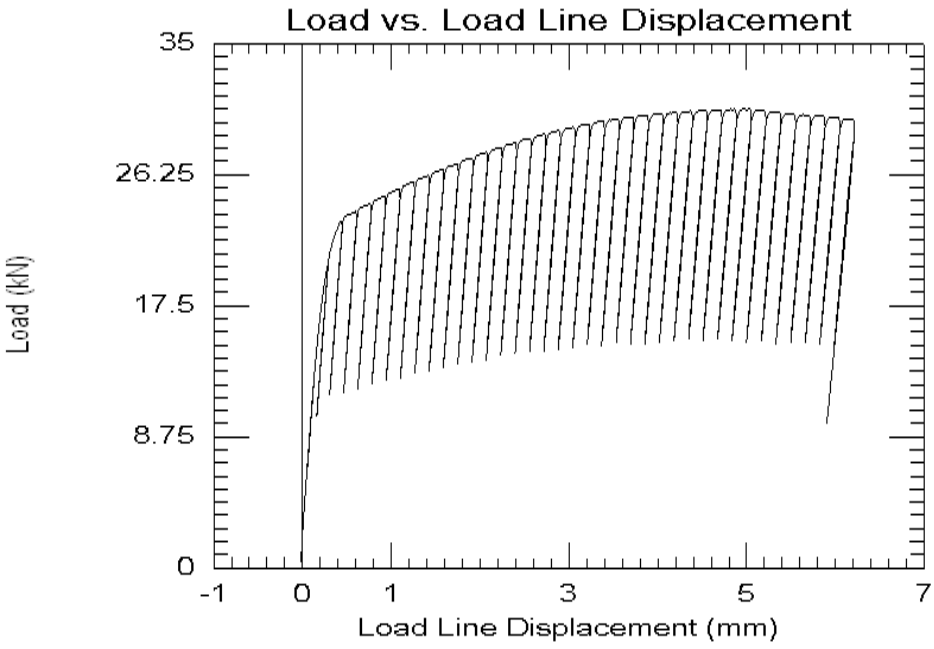

Fig. 4.4 An example of the unloading compliance method

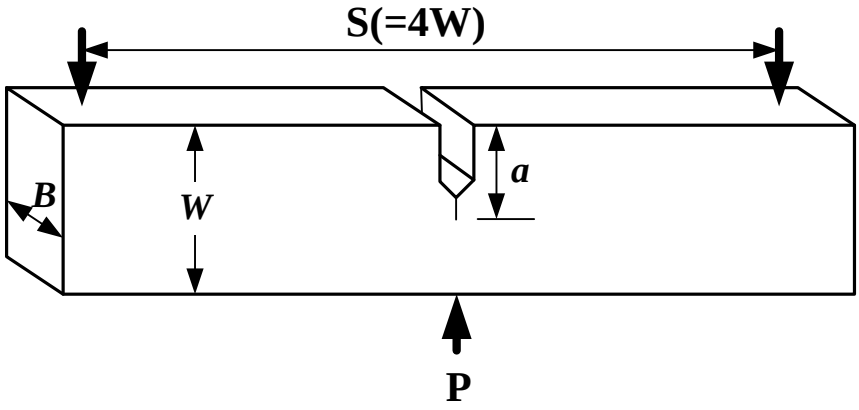

Fig. 4.5 Geometry of the SENB specimen used in fracture test according to specifications ASTM E1820:09

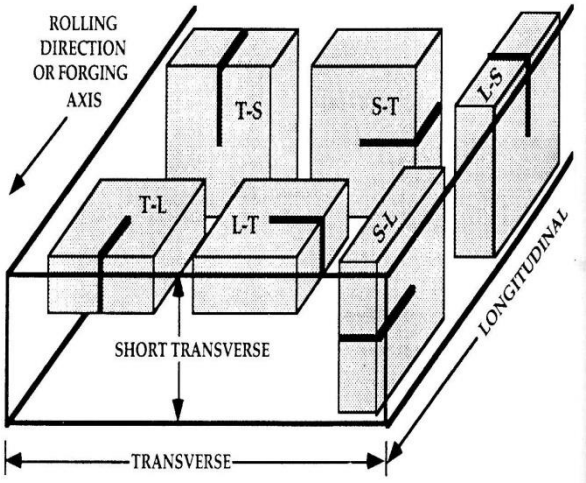

(a)

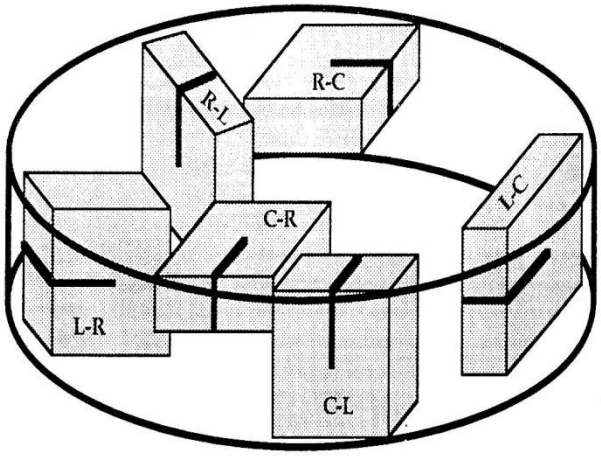

(b)

Fig. 4.6 The ASTM notation for fracture specimens from (a) rolled plate and forgings and (b) disk and hollow cylinders

(a)

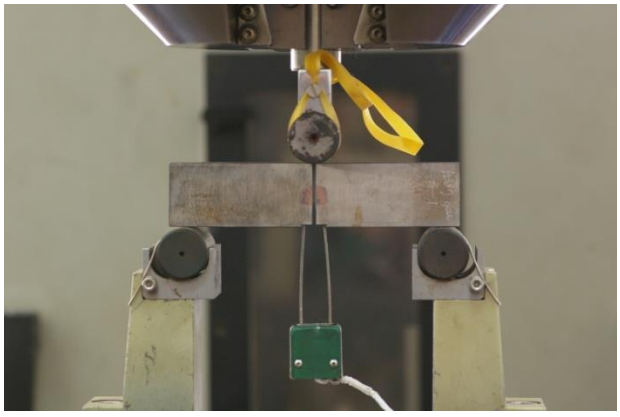

(b)

Fig. 4.7 The equipment and specimen for *J*-integral tests

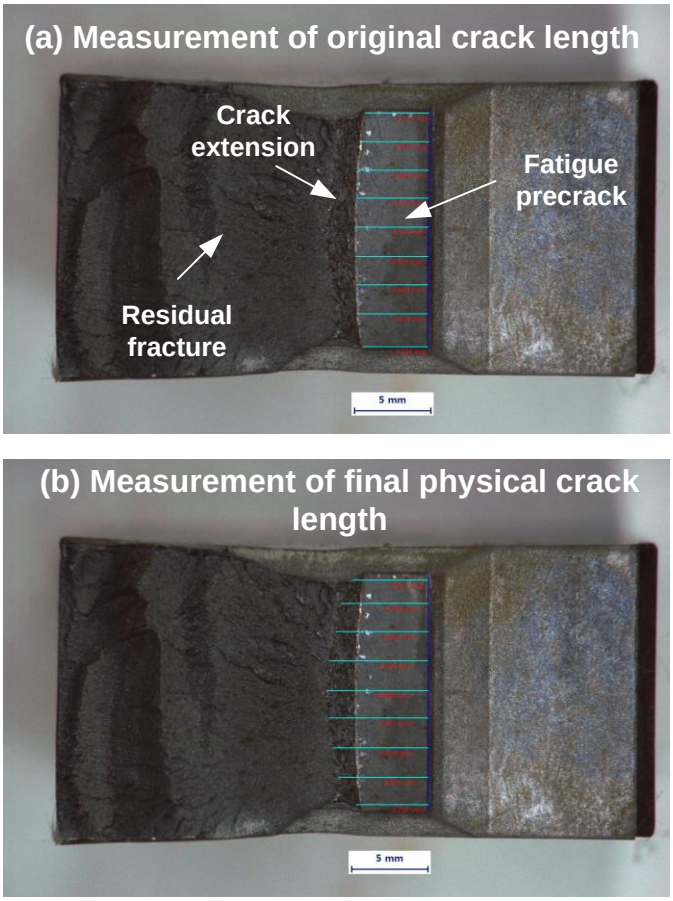

Fig. 4.8 Optical crack size measurement for SCM 21 and API X100: (a) original crack length and (b) final physical crack length

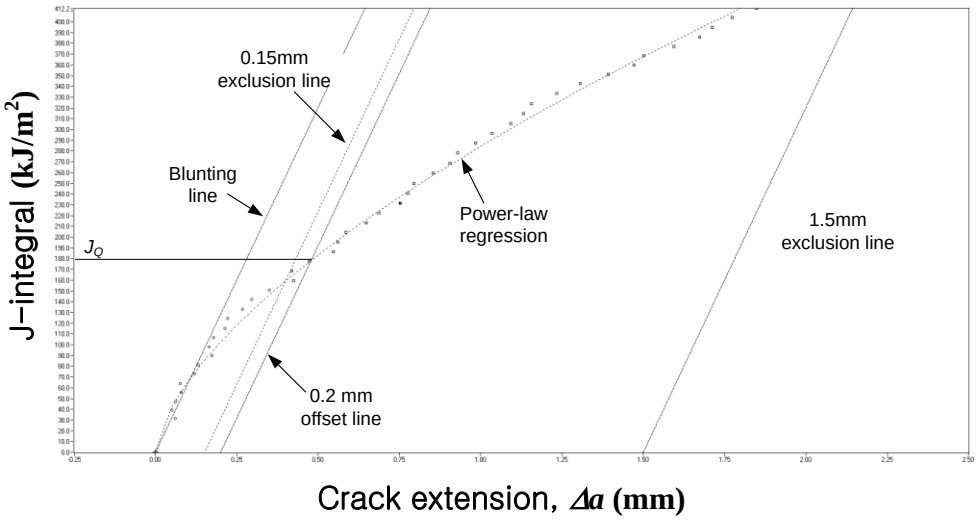

Fig. 4.9 *J-R* curve results

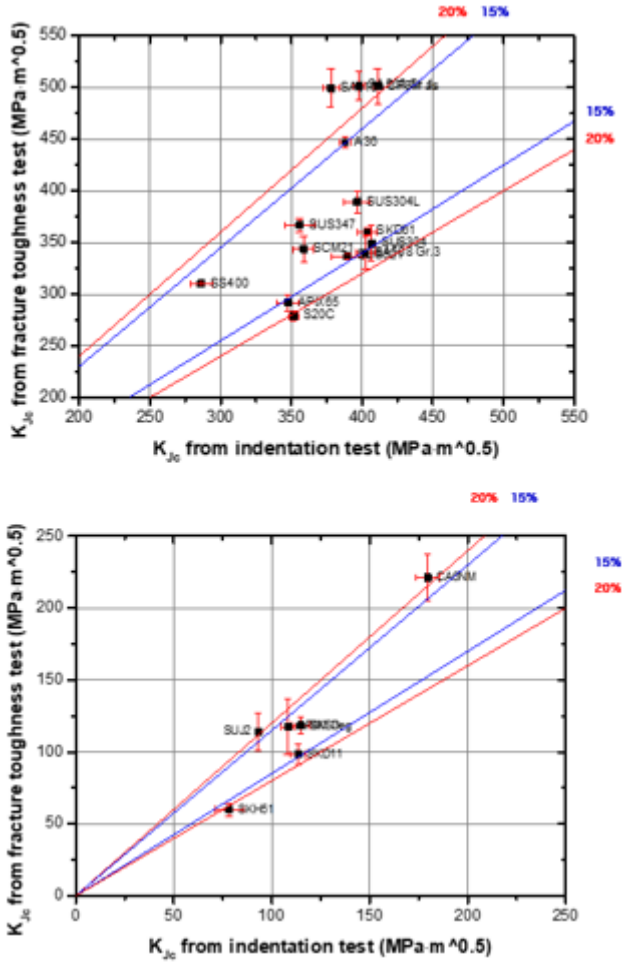

Fig. 4.10 Comparison of fracture toughness results between flat punch indentation tests and J tests

(a) ductile fracture model (b) brittle fracture model

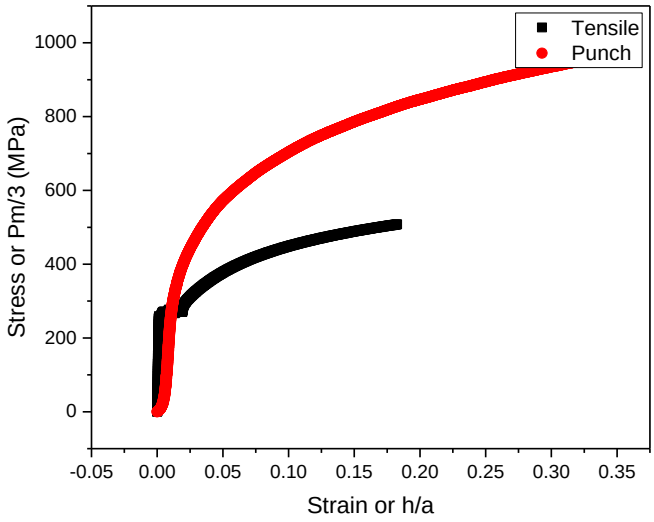

Fig. 4.11 Comparison between normalized flat punch indentation curve and stress strain curve from uniaxial tensile test of SA516

Chapter 5

Extension to Cryogenic environment

Contents

5.1. Introduction

One of the important concerns in discussing fracture properties is the change in properties at cryogenic environment (i.e. relatively low temperatures means under 0℃ temperature. This is related to the phenomenon that ductile fracture and brittle fracture behavior change with temperature. In some metallic materials such as BCC structure in crystallography, the above transitions occurs depending on the temperature, and the temperature at which such transitions occur is called transition temperature. In the case of brittle fracture, unlike ductile fracture, fracture occurs without plastic deformation, and in case of the presence of cracks, fracture occurs as well in an instant due to relatively low fracture toughness. Therefore, in structure integrity, it is important to always maintain the state of the material with a high fracture toughness, the ductile fracture behavior, and keeping the operating environment higher than the transition temperature. These studies have been used from Charpy V-Notch test in the past, and the importance of related studies has increased in recent decades, such as the development of master curve methods such as ASTM E1921 [53] fracture toughness.

In this study, we tried to expand the indentation fracture model to a

cryogenic temperature. In order to perform the indentation test even in a cryogenic environment, we developed chamber type indentation system with a new cooling method and temperature control method. Finally, a instrumented indentation test was performed on the structural material used in the nuclear power plant through developed cryogenic indentation equipment and compared with the master curve test result.

5.2. Development of cryogenic indentation system

In order to develop a cryogenic environment indentation test system, conventional mechanical test methods are studied. The most well-known equipment is a tensile testing device. In the general tensile test apparatus, it was developed to protect the periphery where the specimen is pulled with a hood. Then, liquid nitrogen gas is injected into the hood from the outside to reduce the temperature of the specimen and the surroundings, and the temperature is checked through the temperature sensor inside the hood. The method of controlling the temperature is a method of blocking the injection of liquid nitrogen when the temperature reaches the target temperature. This method has relatively fast cooling and is easy to control the temperature, but there is a limitation in the test method that

tensile test or fracture test can only be performed on one sample.

The Charpy V-Notch impact test adopts a cooling method different from the above method. Since the impact test is performed quickly within 3 seconds of placing the specimen in position, the temperature of the sample is cooled outside the tester, then quickly transferred to the tester before proceeding. In this test, a tank capable of containing the sample is prepared, and liquid nitrogen is added in the tank. After that, put the specimen and saturate it for a certain period of time using the mixed ether to set the desired temperature. This cooling method allows the specimen to be cooled very quickly, and the cooling equipment is very simple and inexpensive. However, considering the test speed of the indentation test, it is very difficult to guarantee the target temperature of the specimen.

Cryogenic testing equipment has also been developed in equipment that evaluates electrical properties rather than mechanical testing methods. One representative equipment is a test device applied to superconducting materials. These devices are used to evaluate the electrical properties of superconductors or to observe the materials at low temperatures. It was developed in such a way that the inside of the equipment is made into a small chamber type, and a small stage was placed inside, and liquid nitrogen was introduced under the stage to take the sample's temperature.

The cooling rate is relatively slow compared to the two conventional methods mentioned above, but it is not slow to achieve cryogenic temperature of small specimens. It is manufactured in a form suitable for small specimens such as superconducting materials, so the equipment has movable function and is designed to relatively easily control temperature by installing a heat source in the chamber.

Considering the cryogenic indentation experiment situation, the following three major issues emerge.

1) When the same method as conventional test equipment is applied to the indentation test, frost is generated on the surface of the specimen. Even if the soaking method is adopted, the temperature change of the specimen cannot be avoided while the indenter approaches the sample and conducts the experiment. Therefore, it is necessary to adopt a method that does not freeze the specimen surface.

2) A delicate temperature control method is required. The indentation test is completed in a relatively short time, but the temperature of the sample must be kept constant during the test.

3) Third, multiple tests should be possible at specific temperatures. For an efficient experiment, the experiment should be carried out by moving

the indentation test position after the experiment even in a cryogenic environment.

We have developed a chamber that reflects the above three considerations.

First, in order to prevent frost on the surface of the specimen, an equipment the type of a chamber that can implement a vacuum was designed. The indentation test machine is designed to be fastened to the upper part of the chamber with ceramic axis, and a rubber ring iss installed at the fastening part to maintain the vacuum. In addition, to prevent the loss of load due to the rubber ring, the load sensor can be located upper part of ceramic axis and a load cell for cryogenic temperature is applied. It is also important to evaluate the temperature of the sample and the cooling section, respectively, for precise temperature control. Therefore, an extra temperature sensor is installed to measure the temperature of the sample and the cooling stage at the same time. As the cooling method, the cooling method used for probe stations used for cooling superconducting materials is adopted. At first, it was designed to install a pipe-through type which liquid nitrogen gas passes, but to maximize cooling efficiency, a tank-type cooling stage is adopted to be quick cooling time as much as possible. Also, a heat chuck is installed

near the surface of the stage to generate heat by electric current, so that it can be heated while being cooled with liquid nitrogen gas. The temperature generated by this chuck is controlled by setting the target temperature higher than the current temperature by using computer software so as to draw a lot of current. Lastly, an automatic position guide is installed to guarantee an accurate indentation position. Since the bind indentation machine can only move up and down, the stage can be moved to perform multiple experiments on one sample. In particular, since the cross roller dovetail slider used at room temperature can be restricted when fine frost occurs on the gears and the mainspring, a linear motion slide guide for cryogenic environment is installed to enable movement with multiple bearings.

Fig. 5.1 to 5.4 are the equipment and devices applied to the cold press system.

5.3. Application

Using the developed cryogenic indentation system, the indentation test in various temperature is performed on materials used in reactor pressure vessels of a nuclear power plant. It is known that the reactor pressure

vessel is exposed to neutrons during in-service period and this makes vessel being embrittlement. Therefore, observing the ductile to brittle transition behavior of these vessels is a very important factor in the assessment of nuclear power plants.

Two sort of low-alloy carbon steel is supplied from Korea Atomic Energy Research Institute (KAERI). The specimens are compact tension and precracked-charpy notch and each materials were used in nuclear power plant. Their chemical compositions are listed in Table 5.1 and the test results are shown as Fig. 5.5 and 5.6 comparing with their master curve results. [99,100]

Table. 5.1 Chemical composition of SA508-Gr.3 / CS50 and JFL

	Chemical composition (%)					
SA508-3 ID:CS50	C	Si	Mn	P	S	Ni
	0.21	0.24	1.36	0.007	0.002	0.92
	Cr	Mo	Al	Cu	V	
	0.21	0.49	0.022	0.03	0.005	

	Chemical composition (%)					
SA508-3 ID:JFL	C	Si	Mn	P	S	Ni
	0.17	0.25	1.44	0.004	0.002	0.75
	Cr	Mo	Al	Cu	V	
	0.20	0.51	0.016	0.01	0.004	

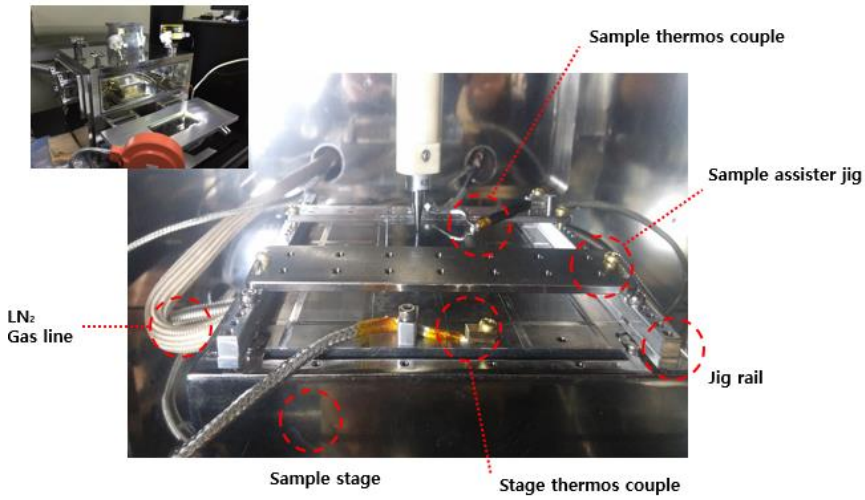

Fig. 5.1 Installed stage and devices in the cryogenic indentation chamber

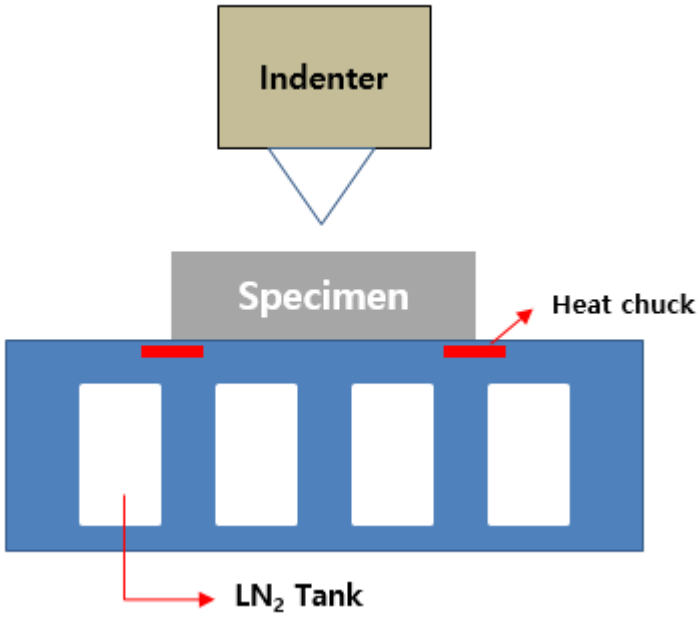

Fig. 5.2 Schematic image of temperature control system

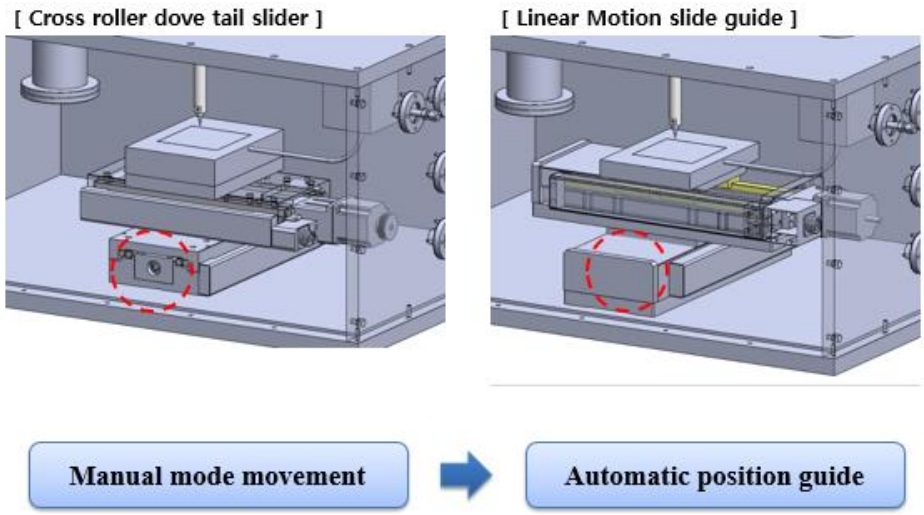

Fig. 5.3 Schematic image of designed stage

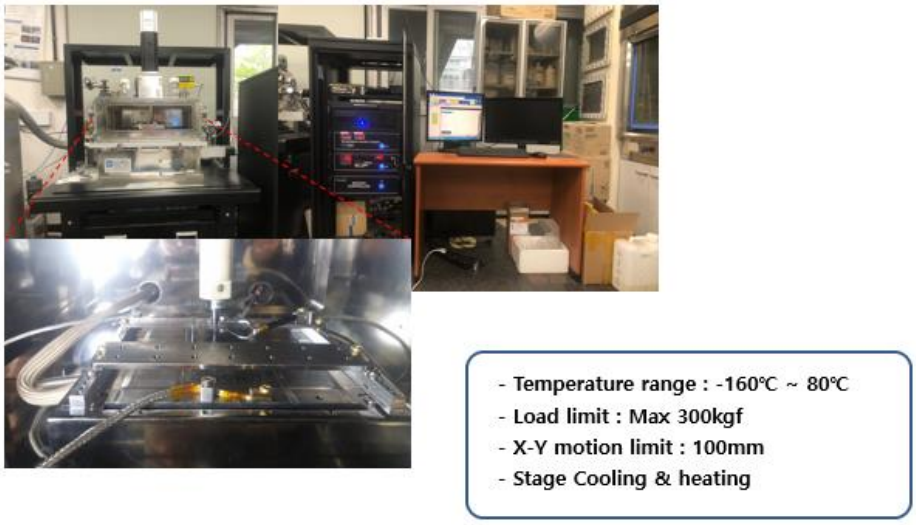

Fig. 5.4 Image of cryogenic indentation system

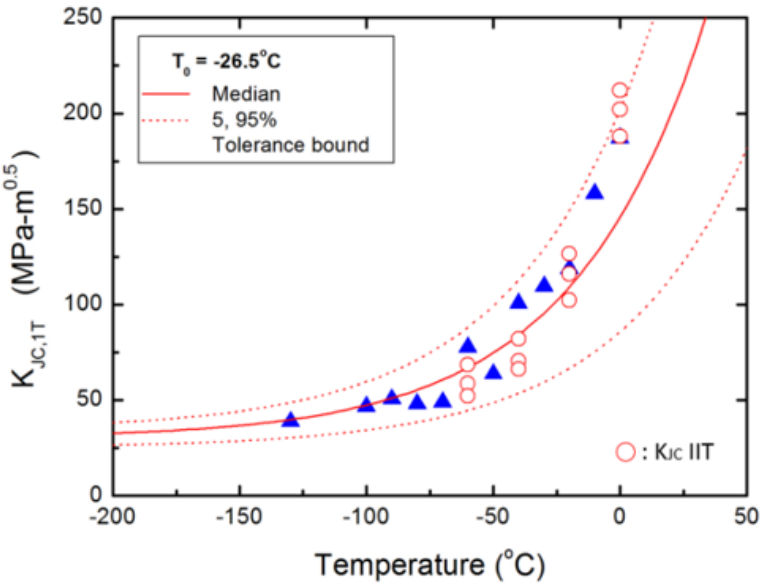

Fig. 5.5 Results of cryogenic indentation test and master curve of CS50

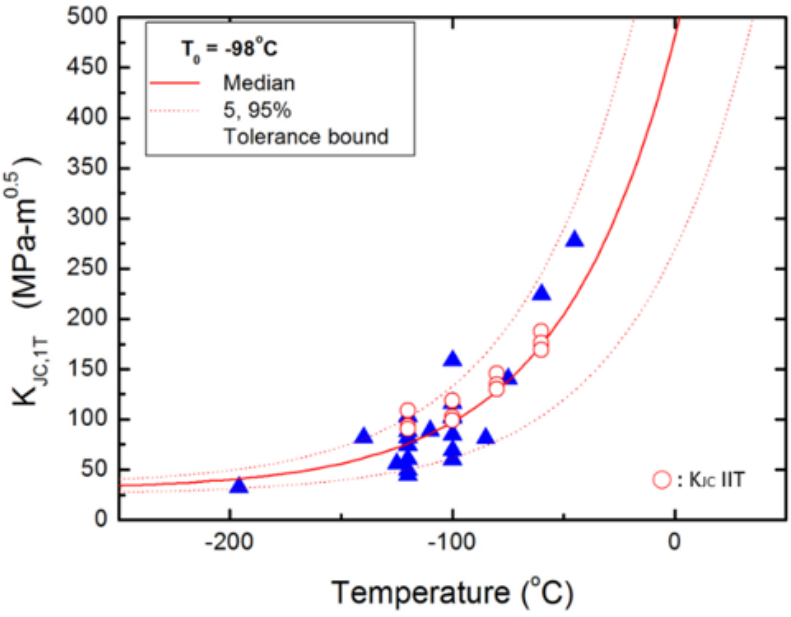

Fig. 5.6 Results of cryogenic indentation test and master curve of JFL

Chapter 6

Conclusion

In this study, an overview of indentation fracture models was presented. By reviewing past models and the methods tried in their studies, a modified model for estimating fracture toughness through a flat punch indentation test was developed. While the previous approach was approached from a somewhat intuitive method and experimental observation, this study was conducted based on mechanical similarities. In addition, as the load-displacement curve of the flat punch indentation was normalized, one normalized curve which is independent of the indenter radius is derived. Through this, it was converted into a load-displacement curve of indenter radius equivalent to 1T thickness in the fracture toughness test. Two models were proposed depending on the fracture behavior. In ductile model, we tried to find the crack initiation point in a cracked round bar fracture studies. Given that the crack propagates when the ligament of cracked round bar specimen is completely filled with the plastic zone, the point at which the plastic zone generated under the flat punch indenter is fully developed was determined as the crack initiation point. In the brittle model, the crack initiation point was determined from the indentation depth in which the size of the plastic zone generated in the indentation test satisfies the small scale yielding condition. To verify models, experimental results are

compared with standard J test results and we confirm that these results match well within 20% error range in both two models. In addition to the fracture toughness, equipment for cryogenic temperature environmental experiments, which are important for evaluating the fracture characteristics, were developed. A temperature control system and a vacuum pump were installed to equipment for the cryogenic indentation test.

Reference

[1] M.F. Doerner and W.D. Nix, J. Mater. Res. **1**, (1986).

[2] W.C. Oliver and G.M. Pharr, J. Mater. Res. **7**, (1992).

[3] W.C. Oliver, G.M. Pharr. *J. Mater. Res.* **19** (2004).

[4] D. Tabor, *The Hardness of Metals*, Clarendon Press (1951).

[5] D.M. Marsh, *Proc. of Res. Soc. of London*, Ser. A **279** (1964)

[6] C.H. Mok, *Exp. Mech.*, **87** (1966).

[7] R.A. George, S. Dinda, A.S. Kasper, *Metals progress*, **30** (1976)

[8] D. Kramer, H. Huang, M. Kriese, J. Robach, J. Nelson, A. Wright, D. Bahr, W.W. Gerberich, *Acta. Mater*., **47** (1999).

[9] J.H. Underwood, G.P. O'Hara, J.J. Zalinka, *Exp. Mech.*, **379** (1986).

[10] H.A. Francis, *Trans. of ASME*, **9** 272 (1976).

[11] F.M. Haggag and G.E. Lucas, *Mater. Tran. A* **14A**, 1607 (1983)

[12] J.S. Field, M.V. Swain, *J. Mater. Res*., **10**, 101 (1995).

[13] A.C. Fischer-Cripps, B.R. Lawn, *Acta Mater.*, **44**, 519 (1996).

[14] J. Alcala, A.E. Giannakopoulos, S. Suresh, *J. Mater. Res.*, **13**, 1390 (1998).

[15] B. Taljat, T. Zacharia, F. Kosel, *Int. J. Solids Struct.*, **35**, 4411 (1998).

[16] J.H. Ahn, D. Kwon, *J. Mater. Res.*, **16**, 3170 (2001).

[17] J.Y. Kim, K.W. Lee, J.S. Lee, D. Kwon, *Surf. Coat. Technol.* **201** (2006).

[18] T.Y. Tsui, W.C. Oliver, G.M. Pharr. *J. Mater. Res*. **11**, 752 (1996).

[19] S. Suresh, A.E. Giannakopoulos. *Acta Mater*. **46**, 5775 (1998).

[20] A. Bolshakov, G.M. Pharr. *J. Mater. Res.* **13**, 1049 (1998)

[21] Y.H. Lee, D. Kwon. *J. Mater. Res*. **17**, 901 (2002).

[22] Y.H. Lee, D. Kwon. *Acta Mater*. **52**, 1555 (2004).

[23] S. Palmquist, *Jernkontorest Ann.* **141**, 300 (1957).

[24] B.R. Lawn BR and J. Wilshaw, *J. Mater. Sci.* **10**, 1049 (1975).

[25] B.R. Lawn, M.V. Swain, *J. Mater. Sci.* **10**, 113 (1975).

[26] B.R. Lawn, E.R. Fuller, *J. Mater. Sci.* **10**, 2016 (1975).

[27] B.R. Lawn, A.G. Evans, D.B. Marshall, *J. Am. Ceram. Soc.* **63** 574 (1980).

[28] F.M. Haggag and R. K. Nanstad, ASTM PVP **170**, 41 (1989).

[29] G.T. Hahn and A.R. Rosenfield, ASTM STP432, American Society for Testing and Materials, **5** (1968): Philadelphia.

[30] T.S. Byun, J.W. Kim, J.H. Hong, J. Nucl. Mater. **252**, 187 (1998).

[31] J.B. Ju, Ph. D. thesis in Seoul National University, (2003).

[32] J.S. Lee, J.-i. Jang, B.W. Lee, Y. Choi, S.G. Lee, and D. Kwon, Acta. Mater. **54**, 1101 (2006).

[33] M. Janssen, J. Zuidema, and R.J.H. Wanhill, Fracture Mechanics 2nd Edition (Spon Press, London and New York, 2004).

[34] A.A. Griffith, *Phil. Trans. A* **221**, 163 (1920).

[35] G.R. Irwin, *Sagamore Research Conference Proceedings* **2**, 289 (1956).

[36] A.A. Wells and D. Post, *Proc. Soc. Exp.* **16**, 69 (1958).

[37] J.R. Rice and G.F. Rosengren, *J. Mech. Phys. Solids* **16**, 1(1968).

[38] H.M. Westergad, *J. App. Mech.* **6**, 49 (1939).

[39] G.R. Irwin, *J. App. Mech.* **24**, 361 (1957).

[40] J.M. Barsom and S.T. Rolfe, Fracture and fatigue control in structures: application of fracture mechanics 3rd (ASTM, 1999).

[41] W.S. Pellini, Proc.: JointUnited States-Japan Symposium on Application of Pressure Component codes, Tokyo, Japan, March 13-15 (1973).

[42] A.A. Wells, Proc. Crack Prop. Sym. **1**, 84 (1961).

[43] T.L. Anderson, Fracture Mechanics 3rd edition (CRC Press, 2005).

[44] G.W. Wellman and S.T. Rolfe, Fracture Mechanics: Sixteenth Sym., ASTM STP 868, 214 (1985).

[45] A.D. Wilson, K. Donald, *Nonlinear Fracture Mechanics: Volume II: Elastic-Plastic Fracture*, ASTM STP 995, 144 (1989).

[46] ASTM Test Method E-399-20: *Standard Test Method for Linear-Elastic Plane-Strain Fracture Toughness K_{IC} of Metallic Materials* (2020).

[47] ASTM Test Method E-1290: *Standard Test Method for Crack-Tip Opening Displacement (CTOD) Fracture Toughness Measurement* (discontinued 2013).

[48] BS 5762, *Methods for Crack Opening Displacement (COD) Testing*, The British Standards Institution (1979).

[49] BS7448, *Fracture Mechanics Toughness Test, The British Standards Institution* (1979).

[50] ASTM Test Method E-1737: *Standard Test Method for J-integral Characterization of Fracture toughness* (discontinued 1998).

[51] ASTM Test Method E-813: *Standard Test Method for J_{IC}, A Measure of Fracture Toughness* ((discontinued 1997).

[52] ASTM Test Method E-1820-20e1: *Standard Test Method for Measurement of Fracture Toughness* (2020).

[53] ASTM Test Method E-1921-19be1: *Standard Test Method for the Determination of Reference Temperature T_o, for Ferritic Steels in the Transition Range* (2019).

[54] T.L Anderson, D. Steinstra, R. H. Dodds, *Fracture Mechanics, 24th*

Volume, ASTM STP 1207, 185 (1985).

[55] M. I. Baskes, *Eng. Fract. Mech.*, **6**, 11 (1974).

[56] K.H. Schwalbe, *Eng. Fract. Mech.*, **9**, 795 (1977).

[57] C.Q. Chen and J.F. Knott, *Met. Sci.*, **15**, 357 (1981).

[58] Z. Cvijovic, M. Vratnica, and K. Geric, *J. Microsc.*, **232**, 589 (2008).

[59] J.M. Barsom and J.V. Pellegrino, *Eng. Fract. Mech.*, **5**, 209 (1973).

[60] V.V. Teleshov and V.G. Kudryashov, *Strength of Materials*, **9**, 967 (1977).

[61] N.V. Oleinik and Ngo Van Kuet, *Probl. Prochn.*, **1**, 72 (1976).

[62] G. Said and S. Tasgetiren, *Eng. Fract. Mech.*, **67**, 345 (2000).

[63] A.A. Baron, *Strength of Materials*, **25**, 556 (1993).

[64] R. Roberts and C. Newton, *WRC Bull.* **299**, 1 (1984).

[65] C.B. Ponton and R.D. Rawlings, *Br. Ceramic Trans. J.*, **88**, 83 (1989).

[66] K.K. Sharma, P.N. Kotru, and B.M. Wanklyn, *App. Surf. Sci.*, **81**, 2 (1994).

[67] M.T. Laugier, *J. Mat. Sci. Letters*, **6**, 779 (1987).

[68] V. Milekhine, M.I. Onsoien, J.K. Solberg, and T. Skaland, *Intermatallics*, **10**, 743 (2002).

[69] N. Perez, *Fracture Mechanics* (Kluwer Academic, 2004).

[70] ISO 14577-1: *Metallic Materials – Instrumented Indentation Test for Hardness and Materials Parameters – Part 1: Test Method* (2002).

[71] ISO 14577-4: *Metallic Materials – Instrumented Indentation Test for Hardness and Materials Parameters – Part 4: Test Method for Metallic and Non-metallic Coatings* (2007).

[72] E.C. Jeon, M.K. Baik, S.H. Kim, B.W. Lee, D. Kwon, *Key Eng. Mater.* **2152**, 297 (2005).

[73] G.E. Dieter, *Mechanical Metallurgy* (McGraw-Hill, New York, 1986).

[74] K.W. Lee, K.H. Kim, J.-Y. Kim, and D. Kwon, *J. Phys. D: Appl. Phys.*, D **41**, 074014 (2008).

[75] S.W. Jeon, K.W. Lee, J.Y. Kim, W.J. Kim, C.P. Park and D. Kwon, *Exp. Mech.*, 57(7), 1013-1025 (2017).

[76] J.Y. Kim, Ph. D. thesis in Seoul National University, (2015).

[77] A.C. Fisher-Cripps, *Introduction to Contact Mechanics 2nd edition* (Springer, 2007).

[78] J.R. Rice and D.M. Tracey, *J. Mech. Phys. Solids*, **17**, 201 (1969).

[79] H.A. Francis, *J. Eng. Mater. Tech.*, **98**, 272 (1976).

[80] J. Lemaitre, *J. Eng. Mater. Tech.*, **107**, 83 (1985).

[81] G.E. Fougere, L. Riester, M. Ferber, J.R. Weertman, and R.W. Siegel,

Mater. Sci. Eng. *A* **204**, 1 (1995).

[82] L.M. Brown and J.D. Embury, *Proc. 3rd Int. Conf. Strength of Metals and Alloy* **1**, 164 (1973).

[83] S.H. Goods and L.M. Brown, *Acta Metall.*, **27**, 1 (1979).

[84] K.W. Lee, Ph. D. thesis in Seoul National University, (2011).

[85] H. Hertz, Eds. Jones, Schott On the contact of elastic solids. Miscellaneous Papers, Macmillan, London (1892)

[86] K.L.Johnson, Contact mechanics. Cambridge University Press, London (1985)

[87] C. J. Peel, P. J. E. Forsyth, Metal Science Journal **7**: 121 (1973)

[88] J.Y. Kim, Ph. D. thesis in Seoul National University, (2015)

[89] M. Scibetta, R. Chaouadi, E. Van Walle, *Int. J. Fract*. **104(2)**, 145 (2000)

[90] J. H. Giovanola and T. Kobayashi, *Eng. Fract. Mech*, **59** (1998).

[91] A. Miller, *Int. J. Pres. Vessels Pip*, **32** (1988).

[92] Y. C. Lu, S.N.V.R.K Kurapati, F. Yang *J. Phys. D: Appl. Phys*. **41** 115415 (2008)

[93] B. Riccardi, R. Mntanari, *Mater. Sci. Eng. A*, **381** (2004).

[94] M. Scibetta, Ph. D. thesis in University of Liege, (1999).

[95] Y.J. Xie, D.A. Hills, *Eng. Fract. Mech.* **75** 1223 (2008)

[96] I. N. Sneddon, *Int. J. Eng. Sci.* **3** (1965).

[97] ASTM Test Method E8-16ae1: *Standard Test Method for Tension Testing of Metallic Materials* (2016)

[98] ASTM Test Method E2248-18: *Standard Test Method for Impact Testing of Miniaturized Charpy V-notch Specimens* (2019)

[99] B.-S. Lee, M-C. Kim, M.-W. Kim, J-H. Yoon, J.-H Hong, *Int. J. Press. Vessels Pip* **85** 593 (2008)

[100] B.-S. Lee, J.-H Hong, W.-J. Yang, M.-Y. Huh, S.-H. Chi, *Int. J. Press. Vessels Pip* **77** 599 (2000)

[101] ISO/TR 29381: *Measurement of Mechanical Properties by an Instrumented Indentation Test – Indentation Tensile Properties* (2008).

[102] S. Timoshenko, J.N. Godier, *Theory of Elasticity, third ed.*, (McGraw Hill, New York, 1951).

초 록

구조 건전성 평가는 구조물이나 부품이 파괴를 방지하기 위해 그 구조물이나 부품의 상태를 평가하는 것인데, 구조물의 건전성을 관리하기 위해, 공학자들은 결함의 유무, 설계 응력, 기계적 특성 등을 파악하고자 한다. 그러나 그 중에서도 가장 중요한 요인은 구조물의 기계적 특성으로 강도, 경도 또는 파괴인성 등이 이에 속한다. 구조물이나 설비의 많은 파손 케이스에 있어, 대다수의 파손은 재료의 열화나 취화에 의해 발생하기 때문에, 구조 건전성 평가 시 가동중인 구조물 재료의 기계적 특성을 평가하는 것이 요구된다.

다양한 기계적 특성 중에서도 균열에 대한 저항성의 척도로 표현되는 파괴인성이 구조 건전성 평가의 파괴 역학 분석에 있어 가장 중요한 특성이다. 그러나, 표준에서 제시하고 있는 파괴인성 시험방법은 복잡한 형상과 시험 절차를 요구하고 있기 때문에 가동중인 구조물에 대해 실험을 수행하기에는 거의 불가능하다. 이런 이유에서 비파괴적인 기법을 통해 운용중인 구조물의 기계적 특성을 평가가 요구되고 또 구조 건전성 평가의 신뢰도를 높이고자 연구가 진행되고 있다.

연속압입시험법은 비파괴적으로 가동 중인 구조물에 실험이 가능하여 다양한 기법들 중에서도 가장 유망한 시험법으로 알려져 있다. 이에, 많은 연구자들이 연속압입시험을 통한 파괴인성 예측 연구를 위해 장비와 이론을 개발하고 있다. 이러한 연구는

처음 군열을 직접적으로 발생시키는데서부터 출발하였으나, 결국 대다수의 금속소재들에서는 균열이 발생하지 않기 때문에, 금속소재들을 대상으로 연구가 확장되었다. 금속소재들에서 압입시험 중 균열이 발생하지 않기 때문에 연구는 각각 기계적인 모델링와 파괴 에너지 모델로 나뉘어져 있으나 두 모델에서 모두 실험적인 관계식이나 많은 가정을 포함할 수 밖에 없는 한계가 있었다.

본 연구에서는 압입시험을 통한 파괴인성 예측 모델을 제안하였다. 과거의 많은 연구들이 있었으나, 실험의 간단함과 파괴역학과의 유사성을 유도할 수 있는 끝이 평평한 플랫 펀치 압입자가 채택되었다. 과거의 플랫펀치 연구에서는 다소 현상적인 측면에서 파괴인성을 예측하고자 하였기 때문에 본 연구에서는 보다 파괴역학적인 관점에서 균열 개시시점을 결정하고자 하였다. 파괴 거동에 따라 모델을 연성 파괴 모델과 취성 파괴 모델로 나누었다. 연성 파괴 모델에는 압입자 하부와 균열 팁 앞에서의 유사한 응력 상태를 연결하기 위해, 플랫 펀치 압입자로 시험을 했을 때 압입자 하부에 발생하는 완전 소성 영역과 균열 앞에서의 소성역이 발생하는 것을 관계 지어 균열 개시 시점을 결정하였다. 취성 파괴 모델에서는 소성이 고려되지 않고, 균열 앞에서의 소성 변형에너지가 최소가 되는 소성역이 소규모 항복 조건이 적용되는 것을 통해 균열 개시시점을 결정하였다.

플랫 펀치 압입자를 사용하면, 압입자의 자기 유사성에 의해 압입자 사이즈에무관한 하나의 일반화곡선을 얻을 수 있고,

그로부터 다른 반지름 사이즈의 하중-변위 곡선을 얻을 수 있다. 그러므로 두 모델에 대해 표준의 파괴인성 시험에 주로 사용되는 1T 두께에 대응하는 압입자 사이즈를 결정하여 이 때의 하중-변위 곡선을 통해 파괴인성을 결정할 수 있다.

제안된 모델을 검증하기 위해 J test 파괴인성 결과와 비교하여 두 모델 모두 20% 내외의 오차 범위를 가지는 것을 확인하였다.

또한, 파괴인성의 주요한 영향인자인 온도 영향을 확인하기 위해 극저온 압입시스템을 개발하였다. 기존의 극저온 환경 시험들을 조사하였고, 이를 바탕으로 극저온 압입시험을 도입하였고, 원자력 발전소 구조물에 쓰인 소재를 수급하여 파괴인성 마스터 커브법의 시험결과와 비교하였다.

주요어: 연속압입시험, 파괴인성, , 플랫펀치, 연성파괴, 취성파괴, 극저온 압입

학번: 2013-20589

LIST OF PUBLICATIONS

I. International Journal

1. **Woojoo Kim**, Kyungyul Lee, Jong-hyoung Kim, Young-Cheon Kim, Dongil Kwon: A Further Study on Knoop Indentation Plastic Deformation for Evaluating Residual Stress, *Korean Journal of Metal and Materials, Vol* 58, No. 8, pp.1-7 (2020)

2. **Woojoo Kim**, Seunghun Choi, Junyeong Kim, Seung-won Jeon, Min-Jae choi, Dongil Kwon : Estimation of Fracture Toughness Using Flat-Ended Cylindrical Indentation, *Metals and Materials International* (2020) (In press) (Online published in 20 June 2020)

3. **Woojoo Kim**, Jung-Jun Lee, Jong Ho Won, Dongil Kwon: Residual Life-Time Evaluation Method Using Instrumented Indentation Test, *Key Engineering Materials, Vol* 810, pp.89-94 (2019)

4. Jong-hyoung Kim, Jinwoo Lee, **Woojoo Kim**, , Jongheon Kim, Seung-Kyun Kang, Dongil Kwon: Characterization of Viscoelastic Behavior of Poly(dimethylsiloxane) by Nanoindentation, *Korean Journal of Metal and Materials, Vol* 57, No. 5, pp.289-294 (2019)

5. Seung-won Jeon, Junyeong Kim, Kyung-Woo Lee, **Woojoo Kim**, Chan-Pyung Park, Dongil Kwon: Estimation of Fracture Toughness of Metallic Materials Using Instrumented Indentation: Critical

Indentation Stress and Strain Model, *Experimental Mechanics, Vol* 57, (2016)

II. International Conference (* indicates speaker)

1. Jun-Yeong Kim, **WooJoo Kim***, Seung-Hun Choi, Dongil Kwon: Estimation of Fracture Toughness of Metallic Materials Using Instrumented Indentation Test, ICM12, May 10-14, Karlsruhe, Germany (2015)
2. Dongil Kwon, Seung-won Jeon, John-hyoung Kim, Ohmin Kwon, **WooJoo Kim**, Xu Huiwen, Kwang-Ho Kim：适合材料力学性能评价的仪器化压痕法的应用, 中国力学大会-2015 (The Chinese Congress of Theoretical and Applied Mechanics 2015), Aug 16-20, Shang-hai, China (2015)

3. **Woojoo Kim***, Junyeong Kim, Seungwon Jeon, Seunghoon Choi, Dongil Kwon: Estimation of fracture toughness property using flat punch indentation test, New Methods of Damage and Failure Analysis of Structural Parts, Nov 1-4, Yokohama, Japan (2016)

4. Kyungyul Lee, Jongho Won, Ohmin Kwon**, Woojoo Kim**, Seunghun Choi, Dongil Kwon: Estimating Degradation of High-temperature-component Materials in Gas Turbine Using Instrumented Indentation Test, IIW6, Jul 1-6, Sapporo, Japan (2018)

5. Jongho Won, **Woojoo Kim**, Sungki Choi, Jun Sang Lee, Dongil Kwon:

Residual Life Time Evaluation Method by Using Instrumented Indentation Test, New Methods of Damage and Failure Analysis of Structural Parts, Sep 10-14, Ostrava, Czech (2018)

6. **Woojoo Kim***, Jong-hyoung Kim, Seunghun Choi, Dongil Kwon: Estimation of fracture toughness of metallic material by using instrumented flat-end shaped indentation test, ECF22, Aug 26-31, Belgrade, Serbia (2018)

7. Seunghun Choi, Jong-hyoung Kim, Sungki Choi, Oh Min Kwon, **Woojoo Kim**, Dongil Kwon, Kwang-Ho Kim, Dongseong Ro: Structure Assessment Using Instrumented Indentation: Strength, Toughness And Residual Stress, IPC2018, Sep 24-28, Calgary, Canada (2018)

8. Seunghun Choi, **Woojoo Kim**, Dongil Kwon: Non-Destructive Evaluation of Toughness usi ng Instrumented Indentation Technique, PVP2019, Jul 14-19, San Antonio, USA (2019)

III. Domestic Conference (* indicates speaker)

1. 안희준, **김우주**, 김영천, 최민재, 권동일: 곡면부 구조물의 건전성 평가를 위한 Wedge 연속압입시험을 이용한 잔류응력 평가, 제27회 첨단구조재료 심포지엄, 11월 14일-15일, KIST 전북분원 복합소재기술연구소 (2013)

2. 안희준, **김우주**, 김영천, 권동일: Evaluation of Residual Stress using Wedge Indenter for Integrity Assessment of Curvature Structure, 2014 Materials Fair, 9월 25일, 서울대학교 (2014)

3. 안희준, **김우주**, 김종형, 김영천, 최민재, 권동일: Wedge 압입 시험기법을 활용한 금속재료의 잔류응력 평가연구, 2014년도 대한금속·재료학회 추계 학술대회, 10월 23일-25일, 강원랜드 컨벤션호텔 (강원도 정선) (2014)

4. **김우주***, 김종형, 이준상, 안희준, 김승규, 권동일: 연속압입시험법을 이용한 잔류응력 측정 기술, 2015 KEPIC-Week, 9월 1일-4일, 경주화백컨벤션센터 (2015)

5. **김우주***, 김준영, 전승원, 권동일: Estimation of Fracture Properties of Metallic Materials Using IIT, 2016년도 대한금속·재료학회 춘계 학술대회, 4월 27일-29일, 경주화백컨벤션센터 (2016)

6. **김우주***, 김준영, 최승훈, 권동일: 원기둥 압입자를 이용한 연속압입시험기반 파괴인성 예측 모델 개발, 2017 KPVP, 11월 23일-24일, 창원 두산중공업 (2017)

7. 권동일, 김종형, **김우주**, 이준상: 산업표준 규격화된 IIT 기술 동향, 2018년도 대한금속·재료학회 춘계 학술대회, 4월 25일-27

일, 제주국제컨벤션센터 (2018)

8. 최승훈, **김우주**, 김준영, 권동일: 플랫펀치 압입자를 이용한 연속압입시험 기반의 파괴인성 평가, KPVP 2018년도 연차학술대회, 11월 22일-23일, 광주 김대중컨벤션센터 (2018)
9. 권동일, 최성기, 권오민, **김우주**: 비파괴적으로 현장 건전성 평가가 가능한 연속압입시험법 : 기계적 물성 및 잔류응력, 2019년도 기계학회 플랜트부문, 5월 23일-24일, 부산 벡스코 (2019)

IV. Patent

1. 국문명 : 연속압입시험법을 이용한 파괴인성 측정방법
    - ✓ 발명자 : 김준영 권동일 김광호 전승원 **김우주** 최승훈
    - ✓ 출원인 : ㈜프론틱스
    - ✓ 출원번호 : 10-2016-0095742
    - ✓ 출원일자 : 2016년 7월 27일
    - ✓ 등록번호 : 10-1707492
    - ✓ 등록일자 : 2017년 2월 10일
    - ✓ 국내출원 및 등록

2. 영문명 : METHOD FOR EVALUATING FRACTURE

TOUGHNESS USING INSTRUMENTED INDENTATION TESTING

- ✓ Inventors : Jun Yeong Kim, Seoul (KR); Dong Il Kwon, Seoul (KR); Kwang Ho Kim, Seongman-si (KR); Seung Won Jeon, Seoul (KR); **Woo Joo Kim**, Seoul (KR); Seung Hun Choi, Seoul (KR)
- ✓ Assignee : Frontics, Inc. (KR)
- ✓ Patent number : US009702798B1
- ✓ Date of Patent : Jul. 11, 2017
- ✓ 미국출원 및 등록